TABLE 1. *DNA hypomethylation on pericentromeric satellite regions and clinicopathological parameters in urothelial carcinomas*

Tissue Specimens	No. Analyzed	No. Hypomethylation (%)	p Value (chi-square test)
Satellite 2			
Histological grade			
G1–2	15	2 (13)	
G3–4	12	9 (75)	0.0012
Invasion depth			
Superficial (pTa, pT1)	11	1 (9)	
Invasive (pT2–4)	16	10 (63)	0.0055
Histological structure			
Papillary	21	6 (29)	
Nodular	6	5 (83)	0.0161
Satellite 3			
Histological grade			
G1–2	15	3 (20)	
G3–4	12	9 (75)	0.0043
Invasion depth			
Superficial (pTa, pT1)	11	2 (18)	
Invasive (pT2–4)	16	10 (63)	0.0228
Histological structure			
Papillary	21	7 (33)	
Nodular	6	5 (83)	0.0297

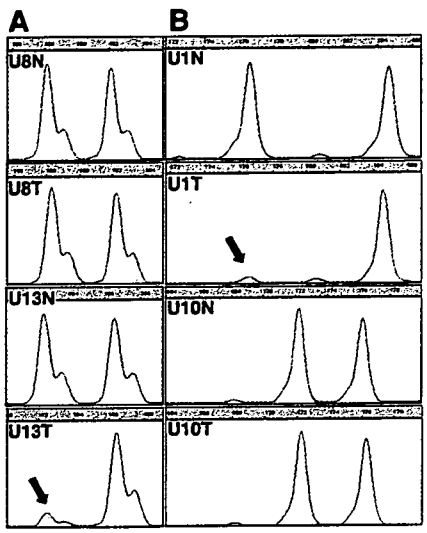

FIG. 2. Examples of results of allelic status analyses in cases of urothelial carcinoma. U8 and U13 DNA samples were amplified for D9S747 (*A*), while U1 and U10 samples were amplified for D9S775 (*B*). Genotypes derived from noncancerous U8N, U13N, U1N and U10N tissues, and corresponding U8T, U13T, U1T and U10T cancerous tissues are shown. Allele size in bp is indicated on top of horizontal axis. In all 4 noncancerous samples PCR products showed polymorphism, indicating that these cases were informative. U8T for D9S747 and U10T for D9S775 were classified as retention of alleles because signal intensity for tumor alleles was not changed significantly relative to matched normal alleles. LOH was identified when signal intensity for tumor allele was decreased by more than 50% relative to matched normal allele, that is in U13T for D9S747 and U1T for D9S775 (arrows).

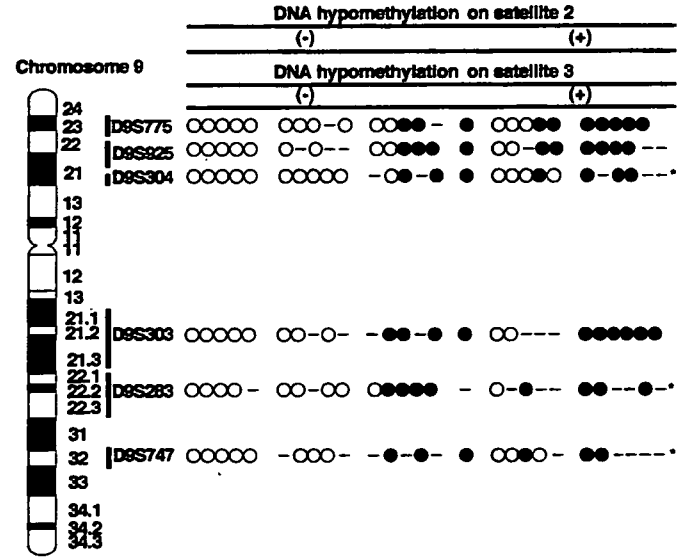

FIG. 3. Allelic status of each locus in urothelial carcinomas. Vertical lines indicate each carcinoma. Open circles indicate retention of 2 alleles. Filled circle indicate LOH. Bar indicates uninformative case. Asterisk indicates replication error. −, negative. +, positive.

TABLE 2. *LOH on chromosome 9 in urothelial carcinomas*

Locus	No. Analyzed	No. Informative	No. LOH (%)
9p			
D9S775	27	24	10 (42)
D9S925	27	21	10 (48)
D9S804	27	22	7 (32)
Any on 9p	27	26	11 (42)
9q			
D9S303	27	20	10 (50)
D9S283	27	18	8 (44)
D9S747	27	17	6 (35)
Any on 9q	27	26	12 (46)
Any on chromosome 9	27	27	14 (52)

hypomethylation on pericentromeric satellite regions significantly correlated with the presence of LOH on at least 1 locus on chromosome 9 in urothelial carcinomas (chi-square test p = 0.0098 and 0.0034 for satellites 2 and 3, respectively, table 4).

DISCUSSION

DNA hypomethylation on satellites 2 and 3 was observed frequently in urothelial carcinomas but it was extremely rare in noncancerous tissues, suggesting that DNA hypomethylation on satellites 2 and 3 is associated with urothelial carcinogenesis. We have previously reported that DNA hypomethylation on satellites 2 and 3 is a frequent and early event during hepatocarcinogenesis,[18] whereas it is rare in colorectal and stomach cancers.[19] These and the current findings suggest that DNA hypomethylation on pericentromeric satellite regions is organ specific during human carcinogenesis. In the current study DNA hypomethylation correlated with tumor aggressiveness (eg histological grade and invasion depth), indicating that it may participate in the malignant progression of urothelial carcinomas. In addition, DNA hy-

TABLE 3: *LOH on chromosome 9 and clinicopathological parameters in urothelial carcinomas*

Parameters	No. Analyzed	No. LOH (%)	p Value (chi-square test)
Histological grade:			
G1–2	15	5 (33)	
G3–4	12	9 (75)	0.0318
Invasion depth:			
Superficial (pTa, pT1)	11	4 (36)	
Invasive (pT2–4)	16	10 (63)	0.1817
Histological structure:			
Papillary	21	8 (38)	
Nodular	6	6 (100)	0.0074

TABLE 4: *DNA hypomethylation on pericentromeric satellite regions and LOH on chromosome 9 in urothelial carcinomas*

Chromosome 9 LOH	Hypomethylation		p Value (chi-square test)
	Neg	Pos	
Satellite 2:			
Neg	11	2	
Pos	5	9	0.0098
Satellite 3:			
Neg	11	2	
Pos	4	10	0.0034

pomethylation was associated more frequently with nodular invasive carcinomas showing an aggressive clinical outcome than with papillary carcinomas. Nodular invasive carcinomas arise from their precursor lesions, that is widely spreading flat carcinoma in situ, and rapidly invading suburothelial tissues, whereas papillary carcinomas usually remain noninvasive for a long period, even after recurrence in the bladder following cystoscopic resection.[13]

LOH on chromosome 9 was detected in more than half of the cases and in these cases rather large regions of 9p and/or 9q were lost, consistent with other reports that loss of an entire chromosome arm is frequent (fig. 3).[11] The observed high incidence of LOH on chromosome 9 in urothelial carcinomas may indicate the existence of tumor suppressor genes important for urothelial carcinogenesis on this chromosome.[11] DNA hypomethylation on satellites 2 and 3 significantly correlated with LOH on chromosome 9 in urothelial carcinomas. After the induction of DNA hypomethylation in cultured cells by treatment with 5-azacytidine, a DNA methyltransferase inhibitor, chromosomal recombination occurred between satellite regions.[3] In patients with ICF syndrome DNA hypomethylation on satellites 2 and 3, and multiradiate chromosomes composed of chromosomes 1, 9 and 16 are characteristic.[2] During hepatocarcinogenesis DNA hypomethylation on satellite 2 significantly correlates with chromosome 1 q-arm copy gain with pericentromeric break points.[8] By analogy with these findings DNA hypomethylation on satellites 2 and 3 could be the underlying molecular background for the frequently observed LOH on chromosome 9 in urothelial carcinomas.

DNMT3b has been identified as a DNA methyltransferase specifically targeting satellites 2 and 3 during mouse development.[20] In human hepatocarcinogenesis over expression of DNMT3b4, a splice variant of DNMT3b that lacks methyltransferase activity and competes with the major variant in normal liver tissues, DNMT3b3, for targeting to pericentromeric satellite regions, results in DNA hypomethylation on these regions.[21] Although further studies are needed to understand the molecular mechanism causing DNA hypomethylation on satellites 2 and 3 during urothelial carcinogenesis, this hypomethylation may have a role in the development and progression of urothelial carcinomas by inducing chromosomal instability. These data highlight the practical significance of correction of DNA methylation status for the prevention and/or therapy of urothelial carcinomas.

REFERENCES

1. Jones, P. A. and Baylin, S. B.: The fundamental role of epigenetic events in cancer. Nat Rev Genet, **3:** 415, 2002
2. Xu, G. L., Bestor, T. H., Bourc'his, D., Hsieh, C. L., Tommerup, N., Bugge, M. et al: Chromosome instability and immunodeficiency syndrome caused by mutations in a DNA methyltransferase gene. Nature, **402:** 187, 1999
3. Kokalj-Vokac, N., Almeida, A., Viegas-Pequignot, E., Jeanpierre, M., Malfoy, B. and Dutrillaux, B.: Specific induction of uncoiling and recombination by azacytidine in classical satellite-containing constitutive heterochromatin. Cytogenet Cell Genet, **63:** 11, 1993
4. Suzuki, T., Fujii, M. and Ayusawa, D.: Demethylation of classical satellite 2 and 3 DNA with chromosomal instability in senescent human fibroblasts. Exp Gerontol, **37:** 1005, 2002
5. Chen, R. Z., Pettersson, U., Beard, C., Jackson-Grusby, L. and Jaenisch, R.: DNA hypomethylation leads to elevated mutation rates. Nature, **395:** 89, 1998
6. Gaudet, F., Hodgson, J. G., Eden, A., Jackson-Grusby, L., Dausman, J., Gray, J. W. et al: Induction of tumors in mice by genomic hypomethylation. Science, **300:** 489, 2003
7. Eden, A., Gaudet, F., Waghmare, A. and Jaenisch, R.: Chromosomal instability and tumors promoted by DNA hypomethylation. Science, **300:** 455, 2003
8. Wong, N., Lam, W. C., Lai, P. B., Pang, E., Lau, W. Y. and Johnson, P. J.: Hypomethylation of chromosome 1 heterochromatin DNA correlates with q-arm copy gain in human hepatocellular carcinoma. Am J Pathol, **159:** 465, 2001
9. Maruyama, R., Toyooka, S., Toyooka, K. O., Harada, K., Virmani, A. K., Zochbauer-Muller, S. et al: Aberrant promoter methylation profile of bladder cancer and its relationship to clinicopathological features. Cancer Res, **61:** 8659, 2001
10. Bornman, D. M., Mathew, S., Alsruhe, J., Herman, J. G. and Gabrielson, E.: Methylation of the E-cadherin gene in bladder neoplasia and in normal urothelial epithelium from elderly individuals. Am J Pathol, **159:** 831, 2001
11. Knowles, M. A.: The genetics of transitional cell carcinoma: progress and potential clinical application. BJU Int, **84:** 412, 1999
12. Sobin, L. H. and Wittekind, Ch.: TNM Classification of Malignant Tumors, 5th ed. New York: John Wiley & Sons, Inc., 1997
13. Friedell, G. H., Parija, G. C., Nagy, G. K. and Soto, E. A.: The pathology of human bladder cancer. Cancer, **45:** 1823, 1980
14. Tagarro, I., Fernandez-Peralta, A. M. and Gonzalez-Aguilera, J. J.: Chromosomal localization of human satellites 2 and 3 by a FISH method using oligonucleotides as probes. Hum Genet, **93:** 383, 1994
15. Hartmann, A., Rosner, U., Schlake, G., Dietmaier, W., Zaak, D., Hofstaedter, F. et al: Clonality and genetic divergence in multifocal low-grade superficial urothelial carcinoma as determined by chromosome 9 and p53 deletion analysis. Lab Invest, **80:** 709, 2000
16. Hartmann, A., Schlake, G., Zaak, D., Hungerhuber, E., Hofstetter, A., Hofstaedter, F. et al: Occurrence of chromosome 9 and p53 alterations in multifocal dysplasia and carcinoma in situ of human urinary bladder. Cancer Res, **62:** 809, 2002
17. Obermann, E. C., Junker, K., Stoehr, R., Dietmaier, W., Zaak, D., Schubert, J. et al: Frequent genetic alterations in flat urothelial hyperplasias and concomitant papillary bladder cancer as detected by CGH, LOH, and FISH analyses. J Pathol, **199:** 50, 2003
18. Saito, Y., Kanai, Y., Sakamoto, M., Saito, H., Ishii, H. and Hirohashi, S.: Expression of mRNA for DNA methyltransferases and methyl-CpG-binding proteins and DNA methylation status on CpG islands and pericentromeric satellite regions during human hepatocarcinogenesis. Hepatology, **33:** 561, 2001
19. Kanai, Y., Ushijima, S., Kondo, Y., Nakanishi, Y. and Hirohashi, S.: DNA methyltransferase expression and DNA methylation of CPG islands and peri-centromeric satellite regions in human colorectal and stomach cancers. Int J Cancer, **91:** 205, 2001
20. Okano, M., Bell, D. W., Haber, D. A. and Li, E.: DNA methyltransferases Dnmt3a and Dnmt3b are essential for de novo methylation and mammalian development. Cell, **99:** 247, 1999
21. Saito, Y., Kanai, Y., Sakamoto, M., Saito, H., Ishii, H. and Hirohashi, S.: Overexpression of a splice variant of DNA methyltransferase 3b, DNMT3b4, associated with DNA hypomethylation on pericentromeric satellite regions during human hepatocarcinogenesis. Proc Natl Acad Sci USA, **99:** 10060, 2002

Staging performance of carbon-11 choline positron emission tomography/computed tomography in patients with bone and soft tissue sarcoma: Comparison with conventional imaging

Ukihide Tateishi,[1,6] Umio Yamaguchi,[2] Testuo Maeda,[1] Kunihiko Seki,[3] Takashi Terauchi,[4] Akira Kawai,[2] Yasuaki Arai,[1] Noriyuki Moriyama[4] and Tadao Kakizoe[5]

[1]Diagnostic Radiology, [2]Orthopedic Division, and [3]Division of Clinical Pathology, National Cancer Center Hospital, [4]Division of Cancer Screening, and [5]President, National Cancer Center, Research Center for Cancer Prevention and Screening, Japan

(Received May 17, 2006/Revised June 21, 2006/Accepted June 26, 2006/Online publication August 14, 2006)

The present study was conducted to compare the diagnostic accuracy between carbon-11 choline (^{11}C-choline) positron emission tomography (PET)/computed tomography (CT) and conventional imaging for the staging of bone and soft tissue sarcomas. Sixteen patients who underwent ^{11}C-choline PET/CT prior to treatment were evaluated retrospectively for staging accuracy. Conventional imaging methods consisted of ^{99m}Tc-hydroxymethylene diphosphonate bone scintigraphy, chest CT and magnetic resonance imaging of the primary site. The images were reviewed and a consensus was reached by two board-certified radiologists who were unaware of any clinical or radiological information using hard-copy films and multimodality computer platform. Tumor stage was confirmed by histological examination and/or by an obvious progression in number and/or size of the lesions on follow-up examinations. Reviewers examining both ^{11}C-choline PET/CT and conventional imaging classified T stage in all patients. Interpretation based on ^{11}C-choline PET/CT, the Node (N) stage was correctly diagnosed in all patients, whereas the accuracy of conventional imaging in N stage was 63%. Tumor Node Metastasis (TNM) stage was assessed correctly with ^{11}C-choline PET/CT in 15 of 16 patients (94%) and with conventional imaging in eight of 16 patients (50%). The overall TNM staging and N staging accuracy of ^{11}C-choline PET/CT were significantly higher than that of conventional imaging ($P < 0.05$). ^{11}C-choline PET/CT is more accurate than conventional imaging regarding clinical staging of patients with bone and soft tissue sarcomas. A whole body ^{11}C-choline PET/CT might be acceptable for imaging studies of tumor staging prior to treatment. (*Cancer Sci* 2006; 97: 1125–1128)

The general diagnostic tools for staging bone and soft tissue sarcomas are clinical examination, magnetic resonance imaging (MRI) and X-ray of the primary tumor site, chest X-ray or computed tomography (CT), and bone scintigraphy.[1]

Positron emission tomography (PET) with [18F]-fluoro-2-deoxy-D-glucose (FDG) has been used in the evaluation of patients with bone and soft tissue sarcomas for grading and therapy monitoring.[2–7] Most of these studies reveal that ^{18}FDG-PET is superior in the assessment of grading and therapy monitoring compared with conventional imaging.

Recently, carbon-11 choline (^{11}C-choline) has been introduced as a new oncological positron-emitting radiopharmaceutical for evaluation of a variety of malignant tumors.[8–11] Choline is an essential component of the cell membrane, and choline uptake may be via a choline-specific transporter protein.[12] Choline kinase, which catalyzes the phosphorylation of choline, is upregulated in malignant cells. Some studies have demonstrated additional gains in diagnostic accuracy using ^{11}C-choline.[13] ^{11}C-choline uptake is significantly higher in malignant tumors than in benign tumors and correlates well with the degree of ^{18}FDG accumulation with the lesion, while the high background activity owing to excretion via urinary tract interferes with evaluation on ^{18}FDG-PET.[14,15] However, the role of ^{11}C-choline PET scan in the staging of bone and soft tissue sarcomas has not been clarified. To fully elucidate the role of ^{11}C-choline PET, the comparison with ^{18}FDG-PET and conventional imaging modalities are needed.

A new-modality PET/CT can improve the localization of tumors and accuracy of staging in patients because anatomic and molecular information can be coregistered precisely.[16] The aim of the current study was to compare the diagnostic accuracy between ^{11}C-choline PET/CT and conventional imaging for the staging of bone and soft tissue sarcomas.

Materials and Methods

Patient. We retrospectively reviewed ^{11}C-choline PET/CT results from September 2005 to March 2006 for patients with bone and soft tissue sarcomas, who subsequently underwent surgical resection, chemotherapy and/or radiotherapy within 2 weeks. ^{11}C-choline PET/CT was performed for initial staging in 12 patients and for restaging of recurrent disease in four patients. The study population consisted of 13 men and three women with a mean age of 44 years (range, 13–75 years). The clinical records of all of the patients were available for review. This study was conducted in accordance with the amended Helsinki declaration and the protocol was approved by the Institutional Review Board (National Cancer Center, Research Center for Cancer Prevention and Screening). All of the patients provided their written informed consent to participate in the present study and to review their records and images.

Radiopharmaceuticals. Carbon-11 choline was synthesized with a commercial module essentially using the method described by Hara and Yuasa.[17] $^{11}CO_2$ was converted to ^{11}C-methyl iodide by $LiAlH_4$/HI reaction. ^{11}C-methyl iodide was trapped in dimethylaminoethanol. After a washing step with ethanol and water, ^{11}C-choline retained on a cation exchange resin was eluted with saline. Radiochemical purity of the solution was evaluated by liquid chromatography radiodetector. The organic solvents were analyzed by gas chromatography. Endotoxin was assayed by the lysosomal acid lipase method.

PET/CT. Scans were acquired with a PET/CT device (Aquiduo; Toshiba Medical Systems, Tokyo, Japan) that consisted of a PET scanner (ECAT HR+; CTI, Knoxville, TN, USA) and 16-section CT scanner (Aquilion V-detector; Toshiba Medical Systems) with a whole-body mode implemented as the standard software. Prior to the ^{11}C-choline PET/CT study, the patients fasted for at least

[6]To whom correspondence should be addressed. E-mail: kuenstrell@nifty.com

doi: 10.1111/j.1349-7006.2006.00288.x

Table 1. Summary of patients and confirmed staging

Patient no.	Diagnosis	SUV	Size (mm)	Staging type	Location	TNM	Metastasis	Grade	Stage
1	Leiomyosarcoma	4.63	110	Initial	Retroperitoneum	T2bN0M1	Soft tissue	High	IV
2	Rhabdomyosarcoma	3.03	60	Initial	Perineum	T2bN1M0	Lymph node	High	IV
3	Pleomorphic malignant Fibrous histiocytoma	15.05	133	Initial	Chest wall	T2bN0M1	Bone, pleura, lymph node	High	IV
4	Leiomyosarcoma	4.10	80	Initial	Retroperitoneum	T2bN0M,P	Lung	Low	IV
5	Osteosarcoma	6.70	110	Initial	Iliac bone	T2N0M1b	Bone, lung	High	IVB
6	Clear cell sarcoma	13.03	80	Initial	Chest wall	T2bN0M1	Bone, lung, pleura, lymph node	High	IV
7	Myxoid liposarcoma	2.15	50	Initial	Leg	T1aN1M0	Lymph node	Low	IVB
8	Osteosarcoma	5.31	110	Initial	Tibia	T2N1M0	Lymph node	High	IV
9	Ewing sarcoma	3.46	95	Initial	Leg	T2bN0M0	N/A	High	III
10	Ewing sarcoma	9.86	102	Initial	Shoulder	T2N0M0	N/A	High	IIB
11	Ewing sarcoma	6.14	16	Initial	Spine	T1N0M0	N/A	High	IA
12	Chondrosarcoma	5.99	110	Initial	Iliac bone	T2N0M1b	Bone	High	IVB
13	Leiomyosarcoma	3.18	50	Restaging	Thigh	T1bN1M1	Bone, soft tissue, lymph node	High	IV
14	Osteosarcoma	4.95	75	Restaging	Jaw	T1N0M1a	Lung	High	IVA
15	Osteosarcoma	3.60	50	Restaging	Femur	T1N0M1b	Lung, bone	High	IVB
16	Alveolar soft part sarcoma	3.60	25	Restaging	Shoulder	T2N0M1	Bone	High	IV

N/A, not applicable; SUV, standardized uptake value; TNM, Tumor Node Metastasis.

6 h. CT was performed from the head to the mid-thigh according to a standardized protocol with the following setting: axial 3.0-mm collimation × 16 modes; 120 kVp; 100 mAs; and a 0.5-second tube rotation, pitch 11.0. Patients maintained normal shallow respiration during the three-dimensional acquisition of CT scans. No iodinated contrast material was administered. Emission scans from the base of the skull to the leg were obtained starting 5 min after the intravenous administration of 350–573 MBq of ^{11}C-choline. The acquisition time for PET was 2 min per table position. Images were reconstructed with attenuation-corrected ordered-subset expectation maximization with two iterations and eight subsets using emission scans and CT data.

Positron emission tomography, CT and coregistered PET/CT images were analyzed with dedicated software (e-soft; Siemens). The initial review of the attenuation-corrected PET images was performed using transaxial, coronal and sagittal planes. The images were reviewed and a consensus was reached by two board-certified radiologists who were unaware of any clinical or radiological information using a multimodality computer platform. ^{11}C-choline uptake was considered to be abnormal when it was substantially greater than the surrounding normal tissue. For ^{11}C-choline PET/CT, tumor sizes and T staging were determined by the CT part of PET/CT. ^{11}C-choline-avid lymph nodes or distant metastases on PET/CT were interpreted as positive for metastases regardless of size. Lymph nodes with abnormal uptake were deemed positive for metastases even when they were smaller than 10.0 mm in short axis nodal diameter. Lung nodules without abnormal uptake but highly suggestive of lung metastases on ^{11}C-choline PET/CT were considered to be positive for metastases. A pixel region of interest (ROI) was outlined within regions of increased ^{11}C-choline uptake and measured on each slice. For quantitative interpretations, standardized uptake value (SUV) was determined according to the standard formula, with activity in the ROI given in Bq per mL/injected dose in Bq per weight (kg). However, time decay correction for whole-body image acquisition was not conducted. A SUV of more than 2.5 was considered to characterize malignancy.

Conventional imaging. Conventional imaging methods, performed within 2 weeks of ^{11}C-choline PET/CT, either before or after, were ^{99m}Tc-hydroxymethylene diphosphonate (HMDP) bone scintigraphy, chest CT and MRI of the primary site. ^{99m}Tc-HMDP bone scintigraphy was performed 2 h after intravenous injection of 740 MBq of ^{99m}Tc-HMDP. Both anterior and posterior whole-body planar images were obtained simultaneously with a dual-headed gamma camera (E.CAM; Siemens). Chest CT was performed using a multidetector scanner (Aquilion V-detector; Toshiba Medical Systems) with the following setting: axial 4.0-mm × 4 modes; 120 kVp, automated electric current; 0.5-second tube rotation; and pitch 5. Images were reconstructed with 10.0-mm slice thickness by means of a standard algorithm. MRI of the primary site was performed using a 1.5 Tesla system (Signa Horizon; GE Medical Systems, Milwaukee, WI, USA or Visart; MRI produced by Toshiba Medical Systems, Tokyo, Japan). Pulse sequences comprised T1-weighted spin echo (SE) images, T2-weighted fast spin echo (FSE) images, as well as post-contrast T1-weighted SE images with fat suppression after injection of contrast material. Pulse sequence parameters and slice orientation varied with the examined anatomic site. The images were reviewed and a consensus was reached by two board-certified radiologists who were unaware of any clinical or radiological information using hard-copy films and multimodality computer platform. The two readers for ^{11}C-choline PET/CT and those for conventional imaging were not the same persons.

Each tumor was staged according to the Tumor Node Metastasis (TNM) classification of the International Union Against Cancer for sarcoma of bone and the American Joint Committee staging protocol for sarcoma of the soft tissue.[18,19] T, N and M stages were assigned for both PET/CT and conventional imaging. T staging was confirmed by pathological evaluation using specimens obtained from surgical resection of the primary tumors. N staging was confirmed by pathological examinations in two patients using specimens obtained from sampling of regional nodes. In terms of extraregional nodes in two patients, nodal staging was confirmed by an obvious progression in number and/or size of the lesions on follow-up examinations. The mean follow-up period was 172 days (range, 44–322 days).

Statistical analysis. All valuables were assessed on a patient-by-patient basis. The McNemar test was used for paired comparisons between ^{11}C-choline PET/CT and conventional imaging. Statistical analysis was performed with the SPSS version 11 software program (SPSS, Chicago, IL, USA).

Results

There were eight bone sarcomas and eight soft tissue sarcomas (Table 1). The primary sites included shoulder ($n = 2$), chest wall

doi: 10.1111/j.1349-7006.2006.00288.x

Table 2. Staging of bone and soft tissue sarcoma

Variables	^{11}C-choline PET/CT	Conventional imaging	P-value
Overall stage			0.023
Correct	15 (94)	8 (50)	
Understaged	1 (6)	8 (50)	
Overstaged	0	0	
N stage			0.041
Correct	16 (100)	10 (63)	
Understaged	0	6 (38)	
Overstaged	0	0	
M stage			0.617
Correct	15 (94)	13 (81)	
Understaged	1 (6)	3 (19)	
Overstaged	0	0	

Note: Data are presented as number (*n*). Numbers in parentheses are percentages. CT, computed tomography; PET, positron emission tomography.

($n = 2$), retroperitoneum ($n = 2$), iliac bone ($n = 2$), leg ($n = 2$), thigh ($n = 1$), perineum ($n = 1$), tibia ($n = 1$), femur ($n = 1$), mandible ($n = 1$) and spine ($n = 1$). Pathological diagnoses were osteosarcoma ($n = 4$), Ewing sarcoma ($n = 3$), leiomyosarcoma ($n = 3$), clear cell sarcoma ($n = 1$), chondrosarcoma ($n = 1$), pleomorphic malignant fibrous histiocytoma ($n = 1$), myxoid liposarcoma ($n = 1$), rhabdomyosarcoma ($n = 1$), and alveolar soft part sarcoma ($n = 1$). Histological grade of tumors was grade 1 ($n = 1$), grade 2 ($n = 1$), grade 3 ($n = 11$) and grade 4 ($n = 3$).

All patients of initial staging had increased ^{11}C-choline uptake of the primary lesion (average maximal SUV ± SD: 5.92 ± 3.68 [range, 2.15–15.05]). Pathological T stages available in patients with initial staging are as follows: T1 ($n = 1$), T1a ($n = 1$), T1b ($n = 1$), T2 ($n = 4$) and T2b ($n = 5$). T stages in patients with restaging were T1 ($n = 2$), T1b ($n = 1$) and T2 ($n = 1$). Tumor size of patients for initial staging was 78.5 ± 34.0 mm (mean ± SD [range, 16.0–133.0 mm]). Both ^{11}C-choline PET/CT and conventional imaging classified the T stage correctly in all patients. Twelve (75%) of the 16 patients had N0 disease. Using ^{11}C-choline PET/CT, the N stage was correctly assigned in all patients, whereas the accuracy of conventional imaging in N stage was 63% ($P = 0.041$, Table 2). Understaging occurred in six patients (38%). Three of these patients (19%) had metastasis of inguinal node whose largest diameter was less than 10.0 mm (Fig. 1). The incidence of distant metastases was high in our study population. Both ^{11}C-choline PET/CT and conventional imaging detected bone metastases in seven patients (44%), lung metastases in five (31%) and pleural dissemination in two (18%, Fig. 2). Using ^{11}C-choline PET/CT, the M stage was correctly assigned in 15 patients (94%), whereas the accuracy of conventional imaging in M stage was 81% ($P = 0.617$, Table 2).

The complete stages of all patients were stage IA ($n = 1$), stage IIB ($n = 1$), stage III ($n = 1$) and stage IV ($n = 13$). TNM stage was correctly assessed with ^{11}C-choline PET/CT in 15 of 16 patients (94%) and with conventional imaging in eight of 16 patients (50%, $P = 0.023$, Table 2). ^{11}C-choline PET/CT assigned an incorrect TNM stage in a patient. This patient was understaged due to small metastatic lung tumor which was not clearly visualized by CT part of ^{11}C-choline PET/CT. Eight patients were understaged by conventional imaging (50%). Of these, skip metastases of soft tissues were identified in two (25%) and small nodal metastases in six (75%). ^{11}C-choline PET/CT correctly determined TNM stage in seven patients (44%) in whom stage derived from conventional imaging was incorrect.

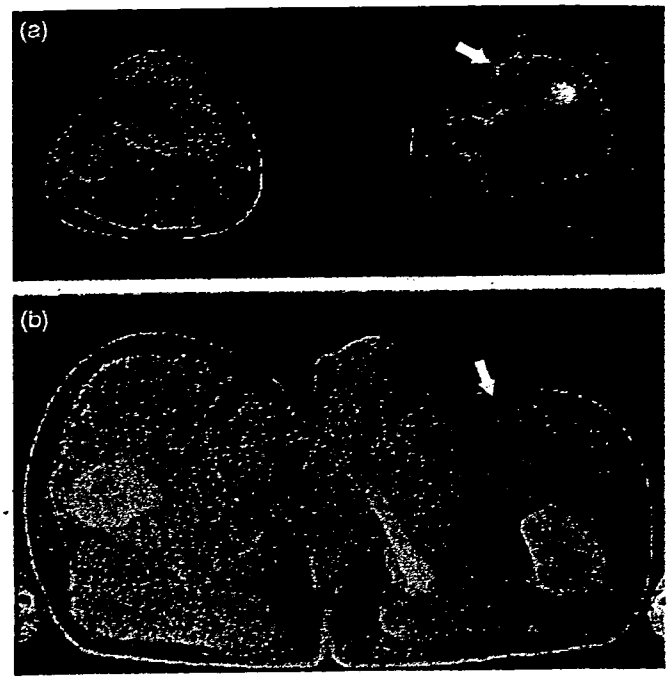

Fig. 1. A 13-year-old boy with osteosarcoma. (a) Transverse ^{11}C-choline positron emission tomography (PET)/computed tomography (CT) image revealed hypermetabolic focus in the proximal portion of the left tibia (arrow). PET/CT findings were verified at histopathological analysis. (b) Abnormal uptake of ^{11}C-choline was also noted in the left inguinal lymph node, which was interpreted as highly suspicious for malignancy (arrow). Subsequent resection revealed metastasis from osteosarcoma.

Discussion

The results of the present study show that ^{11}C-choline PET/CT improves the accuracy of staging in patients with bone and soft tissue sarcomas compared to conventional imaging. Specifically, ^{11}C-choline PET/CT has potentially significant implications for detecting nodal and distant metastases at overall staging. Reports about the efficacy of ^{11}C-choline in the localization and detection of bone and soft tissue sarcomas are still limited.[15] To our knowledge, no study regarding ^{11}C-choline PET/CT for staging bone and soft tissue sarcomas was found. In our study, seven of the 16 patients had skip metastases of soft tissue or nodal metastases detected by ^{11}C-choline PET/CT that were not identified by routine clinical and conventional radiological evaluation.

The ability of PET to depict increased metabolism in malignancies has greatly improved the accuracy in detecting neoplasms.[4] However, compared with conventional imaging studies, use of PET alone results in a lack of substantial detail.[20] The PET/CT device permits sequential acquisition of anatomic CT and functional PET images in a single scanning session. Morphological characterization of scintigraphic lesions by PET/CT resulted in a lower percentage of equivocal interpretations compared with that of conventional imaging. Tumor-detecting PET/CT technology is growing rapidly. However, there are only limited data available on staging of bone and soft tissue sarcomas with PET/CT.

Carbon-11 choline uptake was significantly higher in malignant soft tissue tumors and was due to the high utilization of cell membranes of these lesions. ^{11}C-choline uptake is observed physiologically in the liver, pancreas, kidney and duodenum. ^{11}C-choline is also secreted into phospholipid-rich pancreatic juice in a non-fasting state. A potential advantage of ^{11}C-choline PET/CT might be the assessment of tumors in the skull or retroperitoneum. Blood clearance of ^{11}C-choline is rapid and radioactive distribution

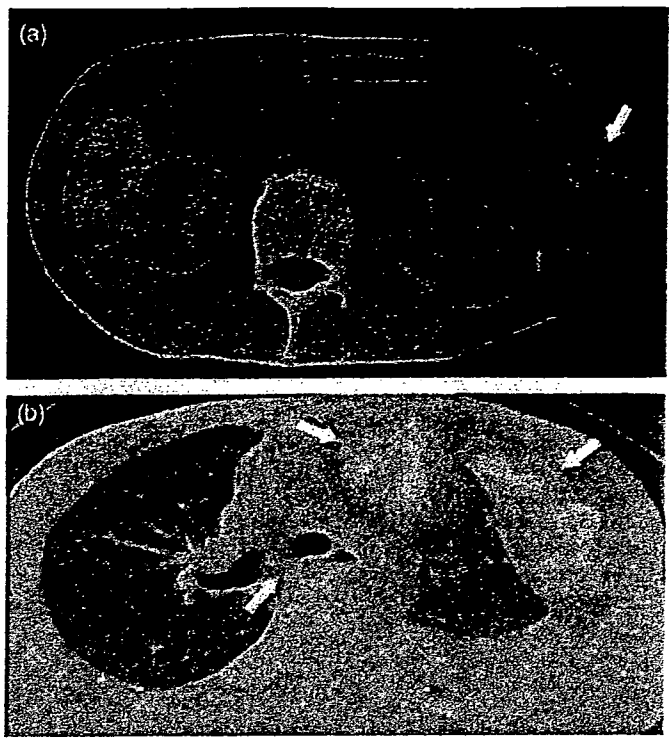

Fig. 2. A 34-year-old man with clear cell sarcoma. (a) Transverse ^{11}C-choline positron emission tomography (PET)/computed tomography (CT) image depicting abnormal uptake in the tumor arising from the left lateral chest wall (arrow). (b) PET/CT image also depicts pleural dissemination and mediastinal lymph node (arrows). Follow-up findings in this patient confirmed the diagnosis.

in tissues is constant in 5 min. The accumulation of ^{11}C-choline in the skull or retroperitoneum is hardly affected by background within the limits of short uptake time. In comparison to ^{18}FDG, physiological background level in the urinary tract is low. This may be due to incomplete tubular reabsorption of the intact tracer, or enhanced excretion of labeled oxidative metabolites like betaine.[12]

Limited resolution of the present generation of ^{11}C-choline PET/CT and the partial volume effect result in failure to detect small lesions. In our study, one patient was understaged due to small metastatic lung tumor, which was not visualized clearly by the CT part of ^{11}C-choline PET/CT. Faint increase in tracer uptake and motion artifact caused by breathing contribute to false negative results. However, the advantage of ^{11}C-choline PET/CT is that the whole-body can be visualized in a single examination. In our study, 50% of patients were understaged by conventional imaging. The inaccuracy of conventional imaging in assessing skip metastases of soft tissues is due to the field of view.

We reported the accurate modality of ^{11}C-choline PET/CT as a non-invasive method for staging in patients with bone and soft tissue sarcomas compared to conventional imaging. Choline is an essential component of the cell membrane, and choline uptake may be via a choline-specific transporter protein. Choline kinase, which catalyzes the phosphorylation of choline, is upregulated in tumor cells.[12] In some types of tumor cells, overexpression of choline-specific transporter protein and choline kinase were identified by *in situ* hybridization.[21] ^{11}C-choline will be phosphorylated by choline kinase as a choline analog and retained in tumor cells.[21] However, the precise pathway of metabolic trapping by tumor cells has not been elucidated, and further studies to clarify the mechanism of imaging by ^{11}C-choline are needed.

Our study has limitations. Most patients in this study had high-grade tumors (88%) and may differ from the patient population of previous studies. Our study was intended to examine the staging prior to treatment; therefore, patient population of high-grade tumors may explain the significant accuracy in overall staging compared to conventional imaging. A study with a larger patient population would clarify the influence of ^{11}C-choline PET/CT on staging. ^{11}C-choline is clearly a sensitive PET tracer for staging patients with bone and soft tissue sarcomas. The short half-life of ^{11}C-choline necessitates the availability of an on-site cyclotron, which causes practical restriction. More specific radiotracers will help overcome this limitation in the future.

In summary, the use of ^{11}C-choline PET/CT in patients with bone and soft tissue sarcomas increases the accuracy of overall staging and N staging compared to conventional staging. Our study suggests that whole-body ^{11}C-choline PET/CT should be the preferred modality for staging in patients with bone and soft tissue sarcomas.

References

1 Reuther G, Mutschler W. Detection of local recurrent disease in musculoskeletal tumors: magnetic resonance imaging versus computed tomography. *Skeletal Radiol* 1990; 19: 85–90.
2 Nieweg OE, Pruim J, van Ginkel RJ *et al.* Fluorine-18-fluorodeoxyglucose PET imaging of soft-tissue sarcoma. *J Nucl Med* 1996; 37: 257–61.
3 Eary JF, Conrad EU, Bruckner JD, Folpe A, Hunt KJ, Mankoff DA, Howlett AT. Quantitative [F-18]fluorodeoxyglucose positron emission tomography in pretreatment and grading of sarcoma. *Clin Cancer Res* 1998; 4: 1215–20.
4 Franzius C, Sciuk J, Daldrup-Link HE *et al.* FDG-PET for detection of osseous metastases from malignant primary bone tumors: comparison with bone scintigraphy. *Eur J Nucl Med* 2000; 27: 1305–11.
5 Schwarzbach MHM, Dimitrakopoulou-Strauss A, Willeke F *et al.* Clinical value of [18-F]fluorodeoxyglucose positron emission tomography imaging in soft tissue sarcomas. *Ann Surg* 2000; 231: 380–6.
6 Ioannidis JP, Lau J. 18F-FDG PET for the diagnosis of soft-tissue sarcoma: a meta-analysis. *J Nucl Med* 2003; 44: 717–24.
7 Tateishi U, Yamaguchi U, Seki K *et al.* Glut-1 expression and enhanced glucose metabolism are associated with tumor grade in bone and soft tissue sarcomas: a prospective evaluation by [F-18]-fluorodeoxyglucose positoron emission tomography. *Eur J Nucl Med Mol Imaging* 2006; 33: 683–91.
8 Hara T, Kosaka N, Shinoura N *et al.* PET imaging of brain tumor with [methyl-^{11}C]choline. *J Nucl Med* 1997; 38: 842–7.
9 Hara T, Kosaka N, Kishi H. PET imaging of prostate cancer using carbon-11-choline. *J Nucl Med* 1998; 39: 990–5.
10 Hara T, Inagaki K, Kosaka N *et al.* Sensitive detection of mediastinal lymph node metastasis of lung cancer with ^{11}C-choline PET. *J Nucl Med* 2000; 41: 1507–13.
11 Torizuka T, Kanno T, Futatsubashi M *et al.* Imaging of gynecologic tumors: comparison of ^{11}C-choline PET with ^{18}F-FDG PET. *J Nucl Med* 2003; 44: 1051–6.
12 Ishidate K. Choline/ethanolamine kinase from mammalian tissues. *Biochim Biophys Acta* 1997; 1348: 70–8.
13 Maeda T, Tateishi U, Komiyama M *et al.* Distant metastasis of prostate cancer: Early detection of recurrent tumor with dual-phase carbon-11 choline positron emission tomography/computed tomography in two cases. *Jpn J Clin Oncol* in press.
14 Zhang H, Tian M, Oriuchi N *et al.* ^{11}C-choline PET for the detection of bone and soft tissue tumours in comparison with FDG PET. *Nucl Med Commun* 2003; 24: 273–9.
15 Tian M, Zhang H, Oriuchi N *et al.* Comparison of ^{11}C-choline PET and FDG PET for the differential diagnosis of malignant tumors. *Eur J Nucl Med Mol Imaging* 2004; 31: 1064–72.
16 Bar-Shalom R, Yefremov N, Guralnik L *et al.* Clinical performance of PET/CT in evaluation of cancer: additional value for diagnostic imaging and patient management. *J Nucl Med* 2003; 44: 1200–9.
17 Hara T, Yuasa M. Automated synthesis of [^{11}C]choline, a positron-emitting tracer for tumor imaging. *Appl radiat Isot* 1999; 50: 531–3.
18 Green FL, Page DL, Fleming ID *et al. AJCC Cancer Staging Manual*, 6th edn. New York: Springer, 2002.
19 Sobin LH, Wittekind C. *UICC TNM Classification of Malignant Tumours*, 6th edn. New York: Wiley, 2002.
20 Franzius C, Daldrup-Link HE, Wagner-Bohn A *et al.* FDG-PET for detection of recurrences from malignant primary bone tumors: comparison with conventional imaging. *Ann Oncol* 2002; 13: 157–60.
21 Uchida T, Yamashita S. Molecular cloning, characterization, and expression in *Escherichia coli* of a cDNA encoding mammalian choline kinase. *J Biol Chem* 1992; 267: 10 156–62.

doi: 10.1111/j.1349-7006.2006.00288.x

Int. J. Cancer: 118, 916–923 (2006)

Promoter hypermethylation of the potential tumor suppressor *DAL-1/4.1B* gene in renal clear cell carcinoma

Daisuke Yamada[1], Shinji Kikuchi[1], Yuko N. Williams[1], Mika Sakurai-Yageta[1], Mari Masuda[1], Tomoko Maruyama[1], Kyoichi Tomita[2], David H. Gutmann[3], Tadao Kakizoe[4], Tadaichi Kitamura[2], Yae Kanai[5] and Yoshinori Murakami[1]*

[1]*Tumor Suppression and Functional Genomics Project, National Cancer Center Research Institute, Tokyo, Japan*
[2]*Department of Urology, Faculty of Medicine, University of Tokyo, Tokyo, Japan*
[3]*Department of Neurology, Washington University School of Medicine, St. Louis, MO, USA*
[4]*Department of Urology, National Cancer Center Hospital, Tokyo, Japan*
[5]*Pathology Division, National Cancer Center Research Institute, Tokyo, Japan*

Renal clear cell carcinoma (RCCC) is a malignant tumor with poor prognosis caused by the high incidence of metastasis to distal organs. Although metastatic RCCC cells frequently show aberrant cytoskeletal organization, the underlying mechanism has not been elucidated. DAL-1/4.1B is an actin-binding protein implicated in the cytoskeleton-associated processes, while its inactivation is frequently observed in lung and breast cancers and meningiomas, suggesting that 4.1B is a potential tumor suppressor. We studied a possible involvement of 4.1B in RCCCs and evaluated it as a clinical indicator. 4.1B protein was detected in the proximal convoluted tubules of human kidney, the presumed cell of origin of RCCC. On the other hand, loss or marked reduction of its expression was observed in 10 of 19 (53%) renal cell carcinoma (RCC) cells and 12 of 19 (63%) surgically resected RCCC by reverse transcription-PCR. Bisulfite sequencing or bisulfite SSCP analyses revealed that the *4.1B* promoter was methylated in 9 of 19 (47%) RCC cells and 25 of 55 (45%) surgically resected RCCC, and inversely correlated with 4.1B expression ($p < 0.0001$). Aberrant methylation appeared to be a relatively early event because more than 40% of the tumors with pT1a showed hypermethylation. Furthermore, *4.1B* methylation correlated with a nuclear grade ($p = 0.017$) and a recurrence-free survival ($p = 0.0036$) and provided an independent prognostic factor ($p = 0.038$, relative risk 10.5). These results indicate that the promoter methylation of the *4.1B* is one of the most frequent epigenetic alterations in RCCC and could predict the metastatic recurrence of the surgically resected RCCC.
© *2005 Wiley-Liss, Inc.*

Key words: tumor suppressor gene; bi-sulfite sequencing; two-hit inactivation; recurrence-free survival rate; independent prognostic factor

Renal cell carcinoma (RCC) accounts for about 2% of human cancers worldwide, with an incidence of 189,000 and a mortality of 91,000 reported in the year of 2000.[1] Renal clear cell carcinoma (RCCC), which represents 75% of all RCC, exhibits frequent metastasis to distant organs without any clinical symptoms. Furthermore, 40–60% of RCCC tumors without metastasis at first presentation eventually develop metastasis as they progress.[2] Finally, metastatic RCCC becomes refractory to any therapeutic approaches, including chemo-, radio-, and hormonal therapies, resulting in a poor prognosis of patients, with a 5-year survival of less than 10%.[3] Thus, understanding the molecular mechanisms of the development and progression of RCCC is a critical issue for controlling this refractory cancer.

Several genetic and epigenetic alterations have been reported in RCCC. The mutation of the *VHL* gene, associated with loss of heterozygosity (LOH) at the gene locus on chromosomal fragment 3p25–p26, was observed in ~50% of sporadic RCCC.[4] Since the *VHL* encodes a component of an E3 ubiquitin ligase that promotes the degradation of hypoxia-inducible factors, loss of VHL function could be involved in angiogenesis, one of the most characteristic features of RCCC.[5] Epigenetic inactivation of the *RASSF1A*[4] gene is also reported frequently in RCCC.[6–8] In addition, promoter methylation and/or aberrant expression of the *E-cadherin* and *beta-catenin* genes are also found at a high incidence in RCCC, suggesting that disruption of cell adhesion and cytoskeleton organization is also involved in RCCC.[9,10] On the other hand, mutation of the *H-*, *K-*, *N-ras* and inactivation of the *TP53* and *RB1* genes are relatively rare events,[11] while inactivation of the *p16/CDKN2A* gene is involved in a small subset of advanced RCCC.[12]

We have reported that the loss of function of the tumor suppressor in lung cancer 1 (TSLC1) protein, an immunoglobulin superfamily cell adhesion molecule, is implicated in a variety of human cancers in their advanced stages.[13–17] In addition, we have demonstrated that TSLC1 directly binds to DAL-1/4.1B, an actin-binding protein, through its 4.1-binding motif. DAL-1 was originally isolated as an expressed fragment of the *4.1B* gene, whose expression was down regulated in adenocarcinoma of the lung.[18] Restoration of DAL-1 expression in nonsmall-cell lung cancer or breast cancer cell lines significantly suppressed cell growth *in vitro*.[18,19] Moreover, loss of 4.1B expression was observed in human breast cancers and meningiomas, suggesting that the *4.1B* gene is an additional target for inactivation in human cancers.[1–21] Interestingly, 4.1B/DAL-1 interacts with spectrin, an actin-binding protein, and over expression results in altered cytoskeleton-associated properties, including cell adhesion and motility.[20]

To analyze the role of TSLC1 and 4.1B in RCCC, we analyzed 55 surgically resected RCCC and 19 cell lines in the present study. While we could not detect loss of TSLC1 expression, we did find significant alterations in *4.1B* gene expression in these tumors. Herein, we demonstrated that hypermethylation of the *4.1B* gene was a frequent event and could provide an independent prognostic factor for metastatic recurrence after completely resected RCCC.

Material and methods

Cell lines

RCC cell lines, Caki-2, SW839, ACHN, 786-O, 769-P, A-704, A-498 and Hs891.T, were obtained from the American Type

Abbreviations: LOH, loss of heterozygosity; NDS, normal donkey serum; PCR, polymerase chain reaction; RCC, renal cell carcinoma; RCCC, renal clear cell carcinoma; RT-PCR, reverse transcription-polymerase chain reaction; SNP, single nucleotide polymorphism; SSCP, single-strand conformation polymorphism; TNM, tumor-node-metastasis.

Grant sponsors: the Ministry of Health, Labor, and Welfare, Japan; the Ministry of Education, Culture, Science, Sports, and Technology, Japan; the Program for the Promotion of Fundamental Studies in Health Sciences of Pharmaceutical and Medical Devices Agency (PMDA), Japan; the Foundation for the Promotion of Cancer Research of Japan; the National Institutes of Health; Grant number: NS41520.

*Correspondence to: Tumor Suppression and Functional Genomics Project, National Cancer Center Research Institute, Tsukiji 5-1-1, Chuo-ku, Tokyo 104-0045, Japan. Fax: +81-3-5565-9535.
E-mail: ymurakam@gan2.res.ncc.go.jp

Received 22 March 2005; Accepted after revision 10 June 2005
DOI 10.1002/ijc.21450
Published online 8 September 2005 in Wiley InterScience (www.interscience.wiley.com).

Culture Collection (Rockville, MD); KMRC-1, KMRC-2, KMRC-3, VMRC-RCW, VMRC-RCZ and Caki-1 cells were from the Japanese Collection of Research Bio-resources (Tokyo, Japan); OS-RC-2, RCC10RGB, TUHR4TKB, TUHR10TKB and TUHR14TKB cells were from the Riken Cell Bank (Tsukuba, Japan). Cells were cultured according to the supplier's recommendations.

Surgical specimens

Fifty-five pairs of cancerous and adjacent noncancerous tissues of RCCC were surgically resected at the National Cancer Center Hospital or the Hospital of the University of Tokyo, after obtaining written informed consent from each patient. Pathological diagnosis was performed or confirmed at Pathology Division, National Cancer Center Research Institute, and the clinicopathological features were determined according to the 1997 Union Internationale Contre le Cancer.[22] Analyses of human materials were carried out according to the institutional guidelines.

Reverse transcriptase-polymerase chain reaction (RT-PCR)

Total cellular RNA was extracted using the RNeasy Mini Kit (QIAGEN, Valencia, CA). By using the SuperScript First-Strand Synthesis System (Invitrogen, Carlsbad, CA), 1 μg of total cellular RNA was reverse-transcribed, and an aliquot was amplified by polymerase chain reaction (PCR), using TITANIUM Taq DNA polymerase (BD Biosciences Clontech, Palo Alto, CA) to obtain a 572-bp fragment of DAL-1 cDNA and a 646-bp fragment of human β-actin cDNA in the same reaction. The primers used for PCR were 5′-GGTGCGGAGGGAGGTCACTGACAAGGAACAG-3′ and 5′-CGCTCCCACATTCATCTGGGTCATAGTCTCCGAG-3′ for DAL-1 (1.0 μM, each) and 5′-GGTGCGGAGGGAGGTCACTGACAAGGAACAG-3′ and 5′-CGCTCCCACATTCATCTGGGTCATAGTCTCCGAG-3′ for β-actin (0.2 μM, each).

Restoration of DAL-1 expression by 5-aza-2′-deoxycytidine

At day 0, 1×10^5 cells were seeded, treated with 5-aza-2′-deoxycytidine (10 μM; Sigma-Aldrich, St. Louis, MO) or PBS for 24 hr on days 2 and 5 and collected on day 8, as reported previously.[23]

Loss of heterozygosity (LOH) analysis

Five DNA fragments containing single nucleotide polymorphisms (SNPs) on 18p11.3, namely IMS-JST067229, IMS-JST031621, IMS-JST082513, IMS-JST143134 and IMS-JST119847, were examined for LOH as described previously.[24]

Bisulfite sequencing

Bisulfite sequencing was performed as described previously.[25] Briefly, genomic DNA was denatured with NaOH (0.3 M) and incubated with sodium bisulfite (3.1 M; Sigma) and hydroquinone (0.8 mM; Sigma), pH 5.0, at 55°C for 20 hr, followed by purification and treatment of DNA with NaOH (0.2 M) for 10 min at 37°C. Modified DNA (100 ng) was subjected to PCR to amplify a 92-bp DNA fragment, using a pair of primers (DAL-1 PR2F: 5′-CGGAGTTTCGGTGTTTTTTGTAATAGG-3′ and DAL-1 PR2R: 5′-GCGCCGCGACGTAAAAACTAAAC-3′). The PCR products were subcloned to confirm the sequence of at least 4 clones for each sample.

Bisulfite single-strand conformation polymorphism (SSCP) analysis

For SSCP analysis, the 92-bp fragments were amplified by PCR using two primers, PR2F and PR2R, the latter of which was end-labeled with Texas Red. The PCR products were diluted 7 times with a loading buffer (90% deionized formamide, 0.01% New Fuchsin and 10 mM EDTA), heat-denatured for 3 min at 95°C, immediately cooled on ice for 3 min and then loaded onto the gel (0.5× MDE™ Gel Solution; BMA, Rockland, ME). Electrophoresis was carried out for 120 min at 20°C, using SF5200 (Hitachi Electronics Engineering, Tokyo, Japan) with cooling systems. The analysis was repeated 3 times using independent PCR products. The criterion for hypermethylation was met when the ratio of the methylated fragments to the unmethylated fragments was more than 0.4.

Immunohistochemistry

Sections (5-μm thick) of formalin-fixed, paraffin-embedded specimens were obtained from the National Cancer Center Hospital. For antigen retrieval, the section was heated for 5 min at 120°C with 1 mM EDTA in an autoclave after de-paraffinization and dehydration. Nonspecific reactions were blocked with 5% normal donkey serum (NDS) in TBS. All sections were incubated with anti-DAL-1 antibody (diluted with 1% NDS in TBS 1:2,000) at 4°C overnight. This rabbit polyclonal antibody against 18 amino acids in the U2 domain of DAL-1 was generated by D. H. Gutmann (unpublished results). The sections were then incubated with a labeled polymer, horseradish peroxidase (DakoCytomation, Glostrup, Denmark), at room temperature for 1 hr, rinsed gently with TBS, covered with 3,3′-diaminobenzidine (DakoCytomation) and incubated for 3 min. All sections were counterstained with hematoxylin. 4.1B expression was determined as "membrane expression" when 4.1B signals were detected along the cell membrane in more than 80% of the cells and as an "aberrant expression" or "no expression" when the majority of the 4.1B signals were observed diffusely in the cytoplasm or were undetected.

Statistical analysis

The Kruskal–Wallis test and Mann–Whitney *U*-test were used to examine the correlation with clinicopathological characteristics. Recurrence-free survival was analyzed by the Kaplan-Meier method and the Log-rank test. Multivariate analysis was carried out using the Cox proportional hazard model. The software Stat View 5.0 (SAS institute, Cary, NC) was used for the analysis. Differences with p values of less than 0.05 were considered significant.

Results

Loss of 4.1B expression in RCC

We initially examined the expression of the *4.1B* gene in normal kidney and 19 RCC cell lines by RT-PCR. As shown in Figure 1*a*, a significant amount of 4.1B mRNA was detected in normal kidney. On the other hand, 10 of 19 (53%) RCC cell lines lacked 4.1B mRNA expression. Next, we analyzed the expression of *4.1B* mRNA in 19 surgically resected RCCC as well as several noncancerous renal tissues from the same patients. Semi-quantitative analysis by RT-PCR revealed that *4.1B* mRNA was absent or markedly reduced in 12 of 19 (63%) of these primary RCCC (Fig. 1*b*). These results suggest that the *4.1B* gene may be a target for inactivation in renal carcinogenesis.

Promoter hypermethylation of the 4.1B gene in RCCC

The *4.1B* gene harbors a typical DNA sequence matching the criteria of a CpG island in its upstream region, exon 1, and the beginning of intron 1. To elucidate the molecular mechanisms underlying the loss of 4.1B expression, we examined the methylation status of the *4.1B* promoter in RCC cells. By using bisulfite sequencing, we had previously determined that hypermethylation of the 14 CpG sites within the 92-bp fragment around the *4.1B* promoter strongly correlates with loss of expression in nonsmall-cell lung cancer cell lines.[24] Bisulfite sequencing of the same fragment revealed that these CpG sites were highly methylated in TUHR10TKB and A704 cells lacking 4.1B expression, whereas they were not methylated in KMRC1 cell expressing a significant amount of *4.1B* transcript (Figs. 2*a* and 2*b*). A similar analysis showed that hypermethylation was observed in 9 of 19 (47%) RCC cell lines, where hypermethylation strongly correlated with loss of 4.1B expression ($p = 0.0004$, Fig. 1*a*). To examine the methylation status of the promoter quantitatively, we analyzed the promoter fragments by SSCP after PCR amplification of the bisul-

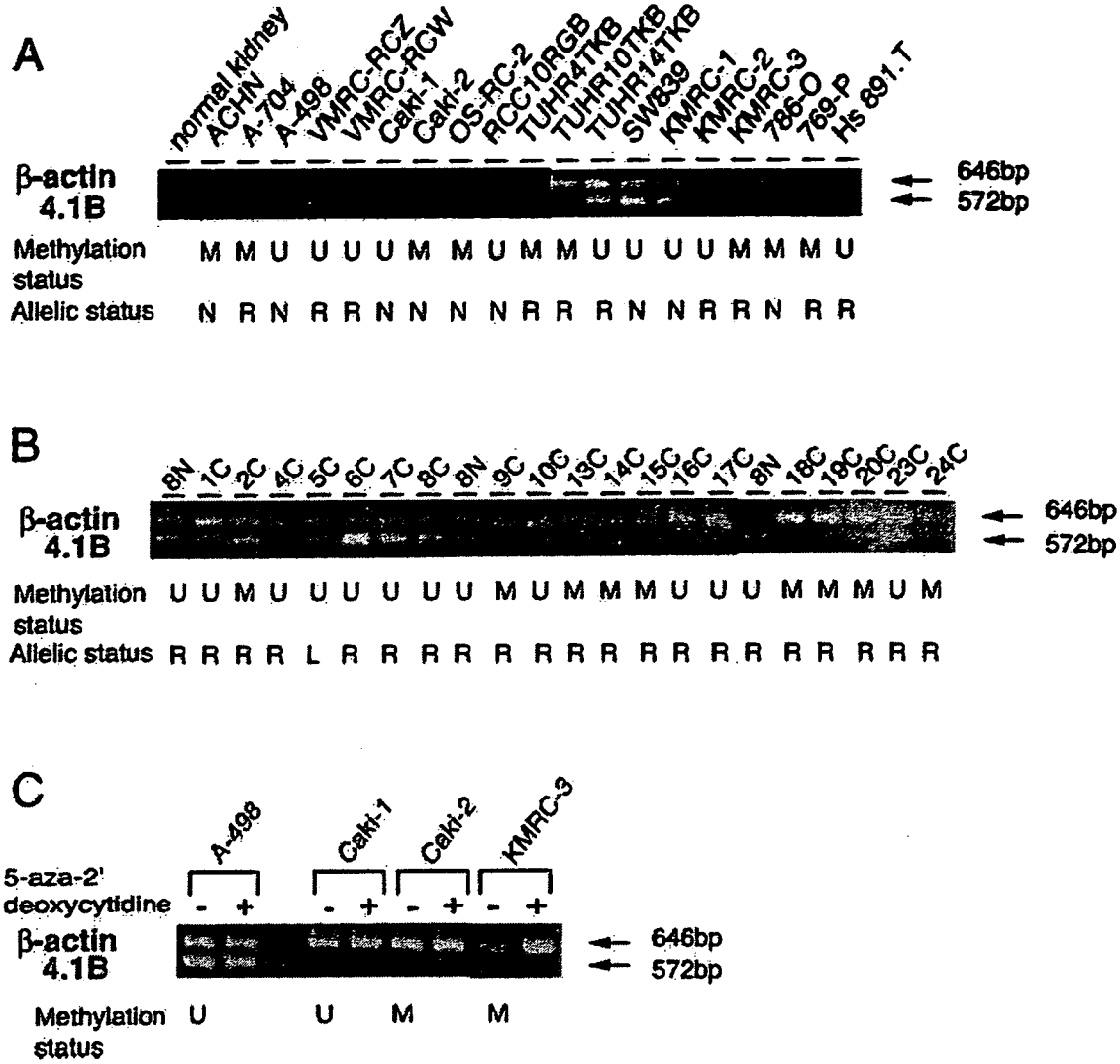

FIGURE 1 – Expression of the *4.1B* gene in RCC. (*a*) and (*b*): RT-PCR analysis of 4.1B and β-actin in RCC cell lines (*a*) and surgically resected RCCC (*b*). C and N in (*b*) indicate cDNA from a cancerous and noncancerous portion of the kidney, respectively. The results of methylation status determined in Figure 2 and allelic status are included as a reference. M and U indicate the hypermethylated and unmethylated promoter of the *4.1B*, respectively. R and L indicate retention and loss of heterozygosity, respectively. N in (*a*) indicates not informative. (*c*): RT-PCR analysis of 4.1B and β-actin in RCC cells treated with 5-aza-2'deoxycytidine (+) or PBS (−).

fite-treated DNA. As shown in Figures 2*a* and 2*c*, clones with known sequences in terms of CpG methylation showed distinct mobility in SSCP analysis, where clone I with no methylation and clone VI with complete methylation showed the slowest and the fastest mobility, respectively. Bisulfite SSCP of RCC cells revealed that TUHR10TKB and A704 cells showed a pattern of hypermethylation, while KMRC1 cell showed a pattern of no methylation, in agreement with the results obtained using bisulfite sequencing (Figs. 2*a* and 2*d*). Next, we examined the methylation status of the *4.1B* in surgically resected RCCC. As shown in Figure 2*e*, DNA from tumors 4C, 5C and 6C showed no methylation, while that from 13C, 14C and 15C showed hypermethylation. DNA from noncancerous renal tissues 4N and 13N showed no methylation. A similar analysis revealed that 25 of 55 (45%) surgically resected RCCC showed hypermethylation. *4.1B* promoter methylation strongly correlated with loss of 4.1B expression in a subset of surgically resected RCCC examined ($p = 0.0063$, Fig. 1*b*, Table I).

FIGURE 2 – Methylation analysis of the *4.1B* promoter. (*a*): Schematic representation of the methylation status of the *4.1B* promoter. A hatched box and an open box indicate a CpG island and exon 1 of the *4.1B*. Vertical bars indicate CpG sites numbered 1–40. Black and white circles represent methylated and unmethylated CpG, respectively. Rows 1–4 indicate the results of independent clones. (*b*): Bisulfate sequencing of the *4.1B* promoter in 3 RCC cells. Sequence traces in each sample correspond to the genomic sequence (−65 bp to −23 bp from the transcription initiation site) shown in the top line. CpG sites, numbered 19–22, are underlined. Asterisks indicate the nucleotides corresponding to methylated cytosine residues at the CpG sites. (*c*)–(*e*): Bisulfate SSCP analyses of the cloned DNA fragments of known sequences (*c*), RCC cells (*d*), and surgically resected RCCC and corresponding noncancerous kidney (*e*). C and N in (*e*) indicate DNA from a cancerous and noncancerous portion of the kidney, respectively. Presence or absence of 4.1B expression determined in Figure 1 is shown as (+) or (−), respectively (*d*) (*e*).

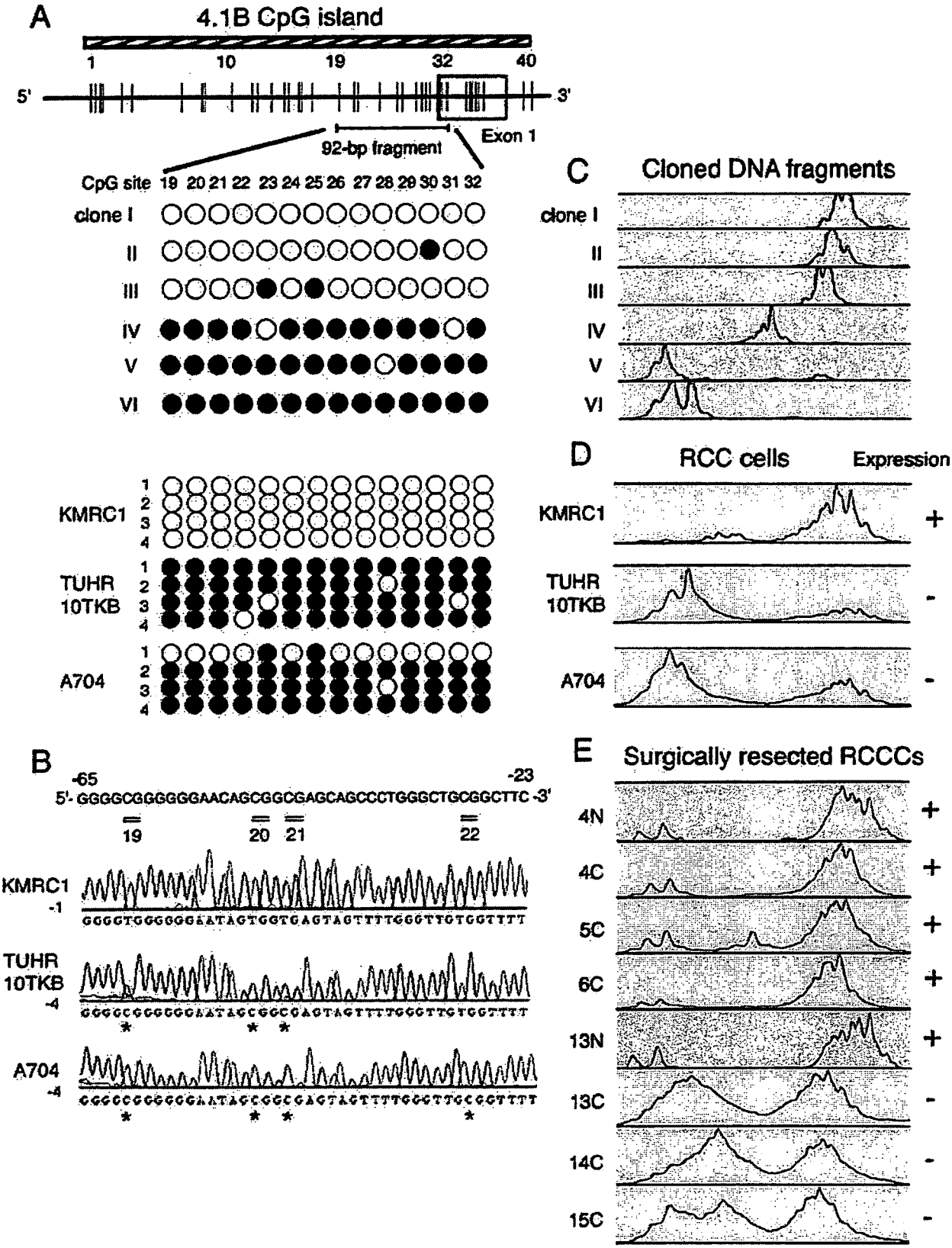
A
4.1B CpG island
1
10
19
32
40
5'
3'
92-bp fragment
Exon 1
CpG site 19 20 21 22 23 24 25 26 27 28 29 30 31 32
clone I
II
III
IV
V
VI
KMRC1
TUHR 10TKB
A704
B
-65
-23
5'- GGGGCGGGGGGAACAGCGGCGAGCAGCCCTGGGCTGCGGCTTC -3'
19
20
21
22
KMRC1 -1
TUHR 10TKB -4
A704 -4
C
Cloned DNA fragments
clone I
II
III
IV
V
VI
D
RCC cells
Expression
KMRC1
TUHR 10TKB
A704
+
-
-
E
Surgically resected RCCCs
4N
4C
5C
6C
13N
13C
14C
15C
+
+
+
+
+
-
-
-

FIGURE 2.

TABLE I – METHYLATION AND EXPRESSION STATUS OF 4.1B AND CLINICOPATHOLOGICAL CHARACTERISTICS IN RCCC

		4.1B Promoter		
	Number of cases	Hypermethylation (%)	No methylation (%)	*p*-value
4.1B expression				
RT-PCR				
Analyzed	19	9 (47)	10 (53)	
Positive	7	1 (14)	6 (86)	
Reduced	2	0 (0)	2 (100)	
Negative	10	8 (80)	2 (20)	0.006[1]
Immunohistochemistry				
Analyzed	20	10 (50)	10 (50)	
Membrane	9	1 (11)	8 (89)	
Aberrant	5	3 (60)	2 (40)	
Negative	6	6 (100)	0 (0)	0.004[2]
Clinicopathological Characteristics				
Analyzed	55	25 (45)	30 (55)	
Age (years)				
60 and older	32	15 (47)	17 (53)	
Under 60	23	10 (43)	13 (57)	NS[1]
Gender				
Male	37	17 (46)	20 (54)	
Female	18	8 (44)	10 (56)	NS[1]
Pathological stage				
I	36	15 (42)	21 (58)	
II	8	4 (50)	4 (50)	
III	8	4 (50)	4 (50)	
IV	3	2 (67)	1 (33)	NS[1]
TNM classification				
pT1a	17	8 (47)	9 (53)	
pT1b	21	8 (38)	13 (62)	
pT2	8	4 (50)	4 (50)	
pT3a	2	1 (50)	1 (50)	
pT3b	5	3 (60)	2 (40)	
pT3c	2	1 (50)	1 (50)	NS[1]
pT4	0	0 (0)	0 (0)	
pN0	54	25 (46)	29 (54)	
pN1,pN2	1	0 (0)	1 (100)	NS[1]
pM0	53	23 (43)	30 (57)	
pM1	2	2 (100)	0 (0)	NS[1]
Nuclear grade				
G1	22	5 (23)	17 (77)	
G2	27	17 (63)	10 (37)	
G3	6	3 (50)	3 (50)	0.017[1]

NS, not significant.
[1]Mann–Whitney *U*-test.–[2]Kruskal–Wallis test.

We then examined the role of promoter methylation in gene silencing of the *4.1B* gene by treating RCC cells with the demethylating agent 5-aza-2′-deoxycytidine. Semi-quantitative RT-PCR analysis revealed that the expression of *4.1B* mRNA following 5-aza-2′-deoxycytidine treatment was only observed in the Caki-2 and KMRC-3 cell lines harboring the hypermethylated *4.1B* promoter, but not in the Caki-1 cell line lacking *4.1B* promoter methylation. These results suggest that *4.1B* promoter methylation is causally related to loss of 4.1B expression (Fig. 1*c*).

LOH analysis of the 4.1B gene

We next analyzed the allelic status of the chromosomal fragment, 18p11.3, around the *4.1B* locus in RCC cells, using 5 highly polymorphic SNP markers. Ten of 19 RCC cell lines showed retention of heterozygosity in at least 1 locus per tumor. Five of these RCC cell lines (A704, TUHR4TKB, TUHR10TKB, KMRC3 and 769-P) harbored a hypermethylated *4.1B* promoter and lacked 4.1B expression. These findings suggest that the *4.1B* gene is inactivated by bi-allelic methylation in some RCC cell lines. In contrast, 9 RCC cell lines did not show heterozygosity at any loci examined, strongly suggesting that one allele of the *4.1B* gene was deleted. Four of these RCC cell lines (ACHN, Caki-2, OS-RC-2, and 786-O) showed promoter hypermethylation with loss of *4.1B* expression, suggesting that the *4.1B* gene was inactivated by 2 hits involving both promoter methylation and LOH. Last, LOH was only observed in 4 of 54 (7.4%) informative cases in surgically resected RCCC, suggesting that bi-allelic methylation may represent the major mechanism to suppress 4.1B expression in primary RCCC.

Aberrant expression of 4.1B protein in surgically resected RCCC

We then examined 4.1B protein expression in human normal kidney as well as primary RCCC, using a polyclonal antibody against U2 domain of human 4.1B.[13] As shown in Figure 3*a*, 4.1B protein was expressed in the baso-lateral membrane of the proximal convoluted tubules, from which RCCC arises. 4.1B protein expression was also found in the basement membrane of the glomeruli, but not in the distal convoluted tubules, Henle's loops or collecting ducts in normal human kidney. An immunohistochemical study of 20 surgically resected RCCC revealed that 9 tumors (45%) demonstrated significant expression of 4.1B protein along the cell membrane, 8 of which (89%) carried the unmethylated *4.1B* promoter (Fig. 3*b*). On the other hand, 6 tumors (30%), all of which (100%) harbored the hypermethylated *4.1B* promoter, showed absence of 4.1B protein expression (Fig. 3*c*). In this regard, loss of 4.1B protein expression significantly correlated with *4.1B* promoter hypermethylation ($p = 0.0040$, Table I). In addition, 5 tumors (25%) showed an aberrant pattern of 4.1B expression, in which weak signals of 4.1B protein were detected

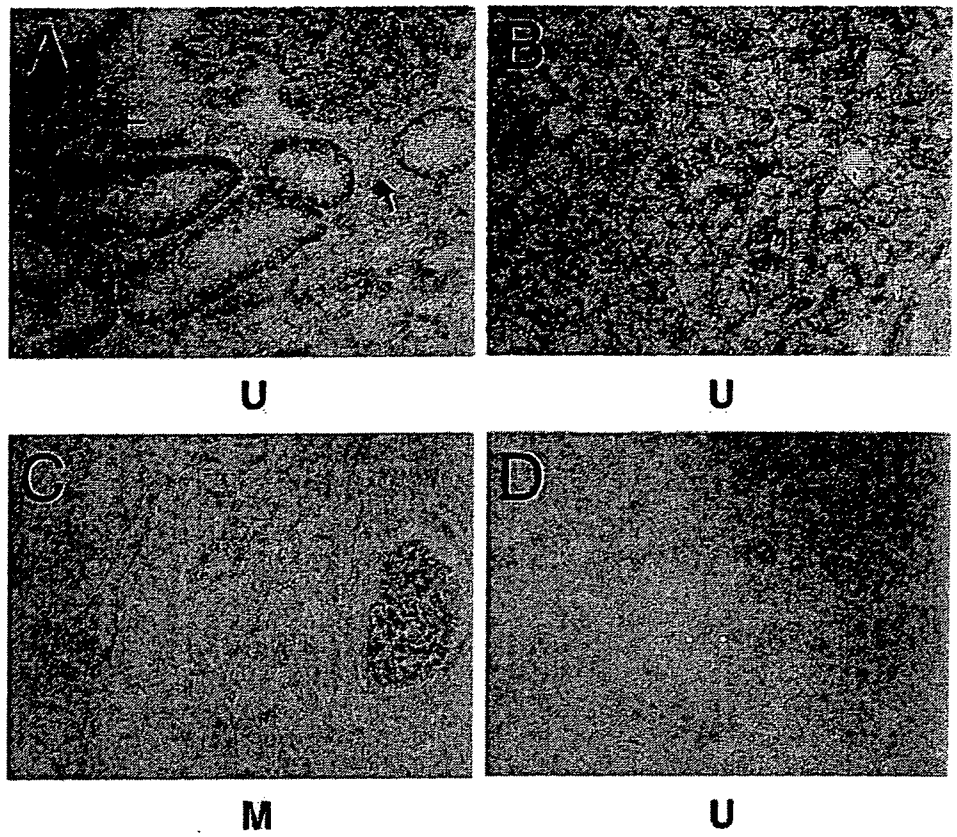

FIGURE 3 – Immunohistochemical analysis of 4.1B protein in human normal kidney (*a*) and surgically resected RCCC (*b*)–(*d*). (*a*) Expression of 4.1B is detected along the basolateral membrane of the proximal convoluted tubules and in the basement membrane of the glomeruli, but not in the distal convoluted tubules (arrows). (*b*): RCCC7C. 4.1B is detected along the cell membrane (membrane expression). (*c*) RCCC19C. 4.1B expression is absent (no expression). The basement membrane of the glomeruli (right) serves as a positive control. (*d*) RCCC5C. 4.1B is present diffusely in the cytoplasm (aberrant expression). M and U indicate tumors with hypermethylated and unmethylated *4.1B* promoter, respectively. Original magnifications, ×400.

diffusely in the cytoplasm, but not at the cell membrane (Fig. 3*d*). Including these tumors with aberrant protein localization, 4.1B expression was abrogated in a total of 11 of 20 surgically resected RCCC (55%).

Clinicopathological features of RCCC with hypermethylation of the 4.1B gene

To understand the clinicopathological significance of the promoter methylation of the *4.1B* gene in surgically resected RCCC, we examined the pathological stage, tumor-node-metastasis (TNM) classification and nuclear grade of the tumors as well as the age and gender of the 55 patients. As shown in Table I, *4.1B* hypermethylation was observed in 15 of 36 (42%) tumors representing stage I and in 8 of 17 (47%) tumors with pT1a, whereas the incidence of hypermethylation did not increase significantly in tumors in more advanced stages. These results suggest that *4.1B* hypermethylation occurs in a subset of tumors as a relatively early event in multi-stage renal carcinogenesis. Correlation of the *4.1B* hypermethylation with lymph node metastasis (pN) or distant metastasis (pM) could not be determined because the great majority of tumors examined were pN0 and pM0 at the time of resection. Interestingly, 4.1B hypermethylation was preferentially observed in tumors with higher nuclear grade ($p = 0.017$). On the other hand, the age and gender of the patients were not correlated with 4.1B hypermethylation.

Hypermethylation of the 4.1B gene correlates with the recurrence-free survival of the RCCC patients

Finally, we examined the significance of *4.1B* methylation as a prognostic factor of metastatic recurrence for RCCC patients. Of 55 patients examined for *4.1B* methylation, 53 patients who received complete surgical resection of RCCC were examined for their prognosis, whereas the other two patients were excluded from the analyses because they harbored metastasis at the time of resection. Kaplan-Meier analysis revealed that the recurrence-free survival of patients with tumors of *4.1B* methylation was significantly shorter than that observed in patients with the unmethylated *4.1B* promoter ($p = 0.0036$, Fig. 4). Furthermore, the multivariate analysis by the Cox hazard model indicated that *4.1B* methylation was an independent prognostic factor, as shown in Table II ($p = 0.038$; relative risk, 10.5).

Discussion

The present study demonstrates that the epigenetic inactivation of the *4.1B* gene is involved in primary RCCC and represents an independent prognostic factor for RCCC patients. Analysis of the expression, methylation and allelic status of the *4.1B* gene revealed that hypermethylation and loss of expression were strongly correlated with each other in both the cell lines and surgically resected RCCC ($p < 0.0001$), as observed in other tumor suppressor genes. The 92-bp fragment including 14 CpG sites that we examined in this study contained a putative transcription start site of *4.1B* gene and a Sp1-binding sequence, which suggests that some methyl-CpG binding proteins might suppress the transcription through interaction with this regulatory motif. While LOH at the *4.1B* locus on 18p11.3 was not frequently observed in surgically resected RCCC, we demonstrated a two-hit inactivation of the *4.1B* in a subset of cell lines by the promoter hypermethylation associated with LOH as well as through bi-allelic hypermethylation. These findings suggest that 4.1B may act as a potential tumor suppressor in human RCCC. It is worth noting that loss of 4.1B expression was also observed in Caki-1 cells and several tumors without *4.1B* methylation (Figs. 1*a* and 1*b*). In this regard, treatment of Caki-1 cells with 5-aza-2′-deoxycytidine did not restore 4.1B expression (Fig. 1*c*). These results suggest that some mechanisms other than promoter methylation, such as histone deacetyla-

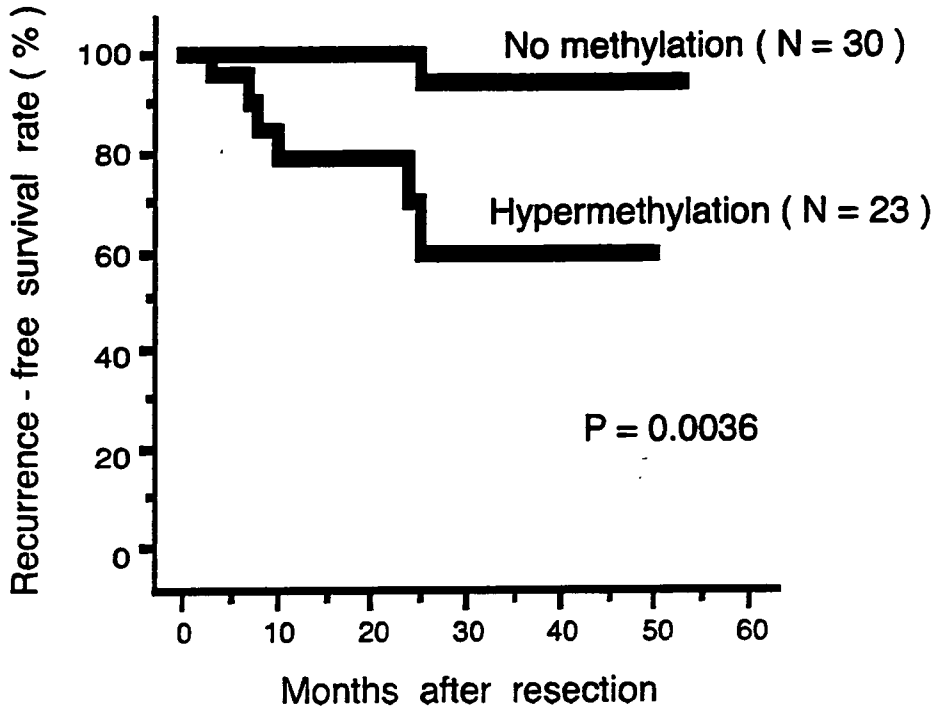

FIGURE 4 – Recurrence-free survival of the patients who received complete resection of RCCC with hypermethylated and unmethylated *4.1B* promoters. Intervals between the primary surgical resection and the metastatic recurrence at the lung, bone, liver, or pancreas are plotted in the Kaplan–Meier analysis. Log-rank *P* is included. N indicate number of cases.

TABLE II – PROGNOSTIC VALUE OF *4.1B* METHYLATION STATUS, PATHOLOGICAL STAGE AND NUCLEAR GRADE FOR RECURRENCE-FREE SURVIVAL IN RCCC

Variable	Kaplan–Meier analysis	Multivariate proportional hazard analysis		
	p-value	Relative risk	95% confidence interval	*p*-value
4.1B methylation status[1] (U *vs.* M)	0.0036	10.5	1.1–97.4	0.038
Pathological stage (I, II *vs.* III, IV)	0.039	4.0	0.83–19.6	0.083
Nuclear grade (1 *vs.* 2, 3)	0.059	1.8	0.18–18.1	0.62

[1]U, no methylation; M, hypermethylation.

tion and deficiency of transcription factors, might be involved in the regulation of 4.1B expression in additional populations of RCCC.

Immunohistochemical studies using anti-4.1B antibody provided information about 4.1B expression, but also 4.1B subcellular localization in primary RCCC. In this study, we found a group of tumors with 4.1B mislocalization, in addition to RCCC tumors lacking 4.1B expression due to promoter hypermethylation. In the tumors with abnormal 4.1B subcellular localization, 4.1B protein was expressed diffusely within the cytoplasm, but not along the cell membrane. Some membrane proteins anchoring DAL-1 to the cell membrane might be inactivated in these cases. This mislocalization might impair the ability of 4.1B to function as a potential tumor suppressor. In this regard, Robb *et al.* have recently shown that growth suppression of meningioma cells by 4.1B/DAL-1 requires proper membrane localization.[26] This aberrant pattern of subcellular distribution in RCCC tumors would be associated with impaired 4.1B function.

By using bisulfite-SSCP, a sensitive and highly quantitative method to detect the methylation status, we found *4.1B* promoter hypermethylation in 25 of 55 (45%) surgically resected RCCC. It has been speculated that the DNA methylation changes are rather rare events in RCCC in comparison with other major malignancies.[27,28] In fact, previous studies have reported that the incidences of hypermethylation in representative tumor suppressor genes, including the *VHL*, *p16/CDKN2A*, *p14/ARF* and *APC* genes, are less than 16% in RCCC.[8,28] However, the extensive analyses have demonstrated that the promoters of the *Timp-3* and *RASSF1A* genes are methylated in 60% and 23–91% of primary RCCC, respectively, suggesting that several critical genes are inactivated frequently by methylation in RCCC as are in many other tumors.[6–8] The incidence of promoter methylation of the *4.1B* (45%) that we have observed in this study is comparable to that of the *Timp-3* and *RASSF1A* genes. Therefore, loss of 4.1B function appears to be strongly selected for the malignant growth of RCCC cells.

It is interesting that the incidence of *4.1B* methylation is more than 40% in tumors with pT1a but does not increase as the T classification advances. The T classification of RCC is determined by the tumor size and the degree of invasion into the renal capsule or vein. In this regard, our findings suggest that *4.1B* promoter hypermethylation is involved in a subset of tumors in a relatively early stage, and is not significantly associated with the tumor size or the degree of invasion at the time of surgical resection. Another interesting result is the significant correlation of *4.1B* promoter hypermethylation with the nuclear grade, which is an indicator of nuclear abnormality of cancer cells ($p = 0.017$). It is worth noting that 4.1B interacts with 14-3-3, a crucial modifier of the G2 checkpoint, by sequestering Cdc2-cyclin B1 complex in the cytoplasm.[29,30] While Robb *et al.* recently suggest that 14-3-3 might not represent the critical 4.1B effector protein,[31] there is emerging data to support a role for 4.1B in the regulation of apoptosis.[19,26]

One of the most serious clinical problems of RCCC is a frequent metastatic recurrence that occurs even after the tumors are completely resected in their early stages. 4.1B is an actin-binding protein involved in actin cytoskeleton organization and actin-mediated processes, including cell motility and adhesion.[19,20] It is possible, therefore, to hypothesize that loss of 4.1B function might be involved in metastasis of RCCC cells to distant organs. Our

findings that *4.1B* promoter methylation is an independent prognostic factor of metastatic recurrence for RCCC patients would support this hypothesis. Furthermore, the observation that the recurrence-free survival of patients with tumors of *4.1B* promoter hypermethylation was significantly shorter than that in patients without *4.1B* promoter hypermethylation ($p = 0.0036$) suggests that 4.1B expression might represent a surrogate marker for this metastatic feature. It should be noted that 2 patients with metastasis at the time of resection, who were excluded from this analysis, also showed *4.1B* promoter hypermethylation in the primary RCCC. In conclusion, our results provide the first demonstration that *4.1B* promoter hypermethylation was involved in the development and/or progression of RCCC and may represent an independent and novel prognostic factor of the metastatic recurrence for RCCC patients.

Acknowledgements

We are grateful to Dr. E. Surace for his technical assistance. This work is supported in part by Grant-in-Aid for the Third-Term Comprehensive Control Research for Cancer from the Ministry of Health, Labor, and Welfare of Japan; a Grant-in-Aid for Special Projects for Cancer Research from the Ministry of Education, Culture, Science, Sports, and Technology of Japan; a Grant from the Program for the Promotion of Fundamental Studies in Health Sciences of Pharmaceutical and Medical Devices Agency (PMDA) of Japan to Y. M. and a Grant from the National Institutes of Health (NS41520) to D.H.G. D. Y., S. K., and M. S.-Y. are recipients of Research Resident Fellowships from the Foundation for the Promotion of Cancer Research of Japan. M. M. is a recipient of Research Fellowships from PMDA.

References

1. Parkin DM, Bray F, Ferlay J, Pisani P. Estimating the world cancer burden: Globocan 2000. Int J Cancer 2001;94:153–6.
2. Motzer RJ, Bander NH, Nanus DM. Renal-cell carcinoma. N Engl J Med 1996;335:865–75.
3. Motzer RJ, Russo P. Systemic therapy for renal cell carcinoma. J Urol 2000;163:408–17.
4. Kondo K, Yao M, Yoshida MS, Kishida T, Shuin T, Miura T, Moriyama M, Kobayashi K, Sasaki N, Kaneo S, Kawakami S, Baba M, et al. Comprehensive mutational analysis of the *VHL* gene in sporadic renal cell carcinoma: relationship to clinicopathological parameters. Genes Chromosomes Cancer 2002;34:58–68.
5. Maxwell PH, Wiesener MS, Chang GW, Clifford SC, Vaux EC, Cockman ME, Wykoff CC, Pugh CW, Maher ER, Ratcliffe PJ. The tumor suppressor protein VHL targets hypoxia-inducible factors for oxygen-dependent proteolysis. Nature 1999;399:271–5.
6. Dreijerink K, Braga E, Kuzmin I, Geil L, Duh FM, Angeloni D, Zbar B, Lerman MI, Stanbridge EJ, Minna JD, Protopopov A, Li J, et al. The candidate tumor suppressor gene, *RASSF1A*, from human chromosome 3p21.3 is involved in kidney tumorigenesis. Proc Natl Acad Sci USA 2001;98:7504–9.
7. Morrissey C, Martinez A, Zatyka M, Agathanggelou A, Honorio S, Astuti D, Morgan NV, Moch H, Richards FM, Kishida T, Yao M, Schraml P, et al. Epigenetic inactivation of the *RASSF1A* 3p21.3 tumor suppressor gene in both clear cell and papillary renal cell carcinoma. Cancer Res 2001;61:7277–81.
8. Dulaimi E, Caceres II, Uzzo RG, Al-Saleem T, Greenberg RE, Polascik TJ, Babb JS, Grizzle WE, Cairns P. Promoter hypermethylation profile of kidney cancer. Clin Cancer Res 2004;10:3972–9.
9. Nojima D, Nakajima K, Li LC, Franks J, Ribeiro-Filho L, Ishii N, Dahiya R. CpG methylation of promoter region inactivates *E-cadherin* gene in renal cell carcinoma. Mol Carcinog 2001;32:19–27.
10. Bilim V, Kawasaki T, Katagiri A, Wakatsuki S, Takahashi K, Tomita Y. Altered expression of β-catenin in renal cell cancer and transitional cell cancer with the absence of *β-catenin* gene mutations. Clin Cancer Res 2000;6:460–6.
11. Michael A, Pandha HS. Renal-cell carcinoma: tumor markers, T-cell epitopes, and potential for new therapies. Lancet Oncol 2003;4:215–23.
12. Kawada Y, Nakamura M, Ishida E, Shimada K, Oosterwijk E, Uemura H, Hirao Y, Chul KS, Konishi N. Aberrations of the *p14 (ARF)* and *p16 (INK4a)* genes in renal cell carcinomas. Jpn J Cancer Res 2001;92:1293–9.
13. Yageta M, Kuramochi M, Masuda M, Fukami T, Fukuhara H, Maruyama T, Shibuya M, Murakami Y. Direct association of TSLC1 and DAL-1, two distinct tumor suppressor proteins in lung cancer. Cancer Res 2002;62:5129–33.
14. Kuramochi M, Fukuhara H, Nobukuni T, Kanbe T, Maruyama T, Ghosh HP, Pletcher M, Isomura M, Onizuka M, Kitamura T, Sekiya T, Reeves RH, *et al. TSLC1* is a tumor-suppressor gene in human non-small-cell lung cancer. Nat Genet 2001;27:427–30.
15. Fukami T, Fukuhara H, Kuramochi M, Maruyama T, Isogai K, Sakamoto M, Takamoto S, Murakami Y. Promoter methylation of the *TSLC1* gene in advanced lung tumors and various cancer cell lines. Int J Cancer 2003;107:53–9.
16. Fukuhara H, Masuda M, Yageta M, Fukami T, Kuramochi M, Maruyama T, Kitamura T, Murakami Y. Association of a lung tumor suppressor TSLC1 with MPP3, a human homologue of *Drosophila* tumor suppressor Dlg. Oncogene 2003;22:6160–5.
17. Surace EI, Lusis E, Murakami Y, Scheithauer BW, Perry A, Gutmann DH. Loss of tumor suppressor in lung cancer-1 (TSLC1) expression in meningioma correlates with increased malignancy grade and reduced patient survival. J Neuropathol Exp Neurol 2004;63:1015–27.
18. Tran YK, Bogler O, Gorse KM, Wieland I, Green MR, Newsham IF. A novel member of the NF2/ERM/4.1 superfamily with growth suppressing properties in lung cancer. Cancer Res 1999;59:35–43.
19. Charboneau AL, Singh V, Yu T, Newsham IF. Suppression of growth and increased cellular attachment after expression of DAL-1 in MCF-7 breast cancer cells. Int J Cancer 2002;100:181–8.
20. Gutmann DH, Donahoe J, Perry A, Lemke N, Karen G, Kittiniyom K, Rempel AS, Gutierrez AJ, Newsham FI. Loss of DAL-1, a protein 4.1-related tumor suppressor, is an important early event in the pathogenesis of meningiomas. Hum Mol Genet 2000;9:1495–500.
21. Perry A, Cai DX, Scheithauer BW, Swanson PE, Lohse CM, Newsham IR, Weaver A, Gutmann DH. Merlin, DAL-1 and progesterone receptor expression in clinicopathologic subsets of meningioma: a correlative immunohistochemical study of 175 cases. J Neuropath Exp Neurol 2000;59:872–9.
22. Bostwick DG, Eble JN, Denis LJ, Murphy GP, von Eschenbach AC. Union International Contre le Cancer (UICC) and the American Joint Committee on Cancer (AJCC) workshop on diagnosis and prognosis of renal cell carcinoma. Cancer 1997;80:973–1001.
23. Veigl ML, Kasturi L, Olechnowicz J, Ma AH, Lutterbaugh JD, Periyasamy S, Li GM, Drummond J, Modrich PL, Sedwick WD, Markowitz SD. Biallelic inactivation of *hMLH1* by epigenetic gene silencing, a novel mechanism causing human MSI cancers. Proc Natl Acad Sci USA 1998;95:8698–702.
24. Kikuchi S, Yamada D, Fukami T, Masuda M, Sakurai-Yageta M, Williams YN, Maruyama T, Asamura H, Matsuno Y, Onizuka M, Murakami Y. Promoter methylation of the *DAL-1/4.1B* predicts poor prognosis in non-small cell lung cancer. Clin Cancer Res, 2005; 11:2954–61.
25. Frommer M, McDonald LE, Millar DS, Collis CM, Watt F, Grigg GW, Molloy PL, Paul CL. A genomic sequencing protocol that yields a positive display of 5-methylcytosine residues in individual DNA strands. Proc Natl Acad Sci USA 1992;89:1827–31.
26. Robb VA, Gerber MA, Hart-Mahon EK, Gutmann DH. Membrane localization of the U2 domain of protein 4.1B is necessary and sufficient for meningioma growth suppression. Oncogene, 2005;24:1946–57.
27. Schulz WA. DNA methylation in urological malignancies (Review). Int J Oncology 1998;13:151–67.
28. Meyer AJ, Hernandez A, Florl AR, Enczmann J, Gerharz CD, Schulz WA, Wernet P, Ackermann R. Novel mutations of the *von Hippel-Lindau* tumor-suppressor gene and rare DNA hypermethylation in renal-cell carcinoma cell lines of the clear-cell type. Int J Cancer 2000;87:650–3.
29. Yu T, Robb VA, Singh V, Gutmann DH, Newsham IF. The 4.1/ezrin/radixin/moesin domain of the DAL-1/protein 4.1B tumor suppressor interacts with 14-3-3 proteins. Biochem J 2002;365:783–9.
30. Osada H, Tatematsu Y, Yatabe Y, Nakagawa T, Konishi H, Harano T, Tezel E, Takada M, Takahashi T. Frequent and histological type-specific inactivation of 14-3-3σ in human lung cancers. Oncogene 2002; 21:2418–24.
31. Robb VA, Li W, Gutmann DH. Disruption of 14-3-3 binding does not impair protein 4.1B growth suppression. Oncogene 2004;23: 3589–96.

Review Article

Development and progression of urothelial carcinoma

Tadao Kakizoe

President, National Cancer Center, Tsukiji 5-1-1, Chuo-Ku, Tokyo 104-0045, Japan

(Received April 26, 2006/Accepted May 11, 2006/Online publication July 6, 2006)

Urothelial carcinomas are well known to feature multifocal development in the urinary tract, both synchronously and asynchronously. This phenomenon can be explained by either seeding of cancer cells in the urinary tract or field cancerization. As there are two characteristic morphological patterns of urothelial carinomas, papillary and nodular, published papers were here reviewed to understand the development and progression of urothelial carcinoma regarding multifocality due to seeding or field changes with reference to the type of urothelial carcinoma. From animal experiments using rats, mice and dogs treated with *N*-butyl-*N*-(4-hydoroxybutyl) nitrosamine, and from pathological observation of human cystectomy specimens on step-sectioning and molecular analysis, nodular carcinomas appear to either develop via papillary carcinomas or *de novo*. Clinical aspects of multifocal tumor development are outside of the scope of this review, although an understanding of the mechanisms underlying multifocality and the papillary/nodular morphological relationship is important to determine follow-up strategies for patients treated for primary urothelial carcinomas and for reconstruction of the urinary tract after cystectomy. (*Cancer Sci* 2006; 97: 821–828)

The urothelium (also known as the transitional cell epithelium) covers the luminal surface of almost the entire urinary tract, extending from the renal pelvis, through the ureter and bladder, to the proximal urethra. Typically it is composed of three to seven layers of cells, that is, basal cells, intermediate cells and superficial cells. The superficial cells are large and binucleated, with a flat characteristic shape leading to the term 'umbrella cell'. Their luminal surfaces are covered with an asymmetric unit membrane, which functions as the permeability barrier between the urine and blood vessels in the urothelium.[1]

Worldwide, there are approximately 336 000 new cases of urothelial carcinoma and 132 000 deaths annually.[2] The majority of lesions are bladder carcinomas, and urothelial carcinomas of the renal pelvis and ureter account for only approximately 7% of the total.[3] In Japan and western countries, more than 90% of bladder carcinomas are urothelial carcinomas, and squamous cell carcinomas and adenocarcinomas are rare. Risk factors include tobacco smoking, occupational exposure to aromatic amines, consumption of arsenic-laced water, radiation therapy of neighboring organs and chemotherapeutic drugs such as alkylating agents. In contrast, in Egypt, where the dominant etiology is schistosomiasis infection, squamous cell carcinomas are the most prevalent bladder carcinoma. Here the focus of attention is urothelial carcinoma in its papillary and nodular forms. Squamous cell carcinoma and the clinical relevance of metaplasia will not be covered.

Multifocal development of urothelial carcinomas

The clinical aspects of multiple urothelial carcinomas need to be emphasized:[4]

1 There are patients in which lesions in the renal pelvis, ureter and bladder are observed simultaneously (Figs 1a, 2).

2 When standard nephrectomy is performed for renal pelvic and ureteral carcinomas, approximately one-third of the lower ureter is left intact. In this remaining ureter, urothelial carcinomas develop subsequently in 20–50% of the patients (Fig. 1b). Consequently, at the present time, the state of the art surgery for renal pelvic and/or ureteral carcinomas is total nephroureterectomy, including removal of a small portion of the bladder with the ureteral orifice (bladder cuff) in the affected side.

3 Even if total nephroureterectomy is carried out, however, 15–50% of patients exhibit subsequent carcinomas in the bladder (Fig. 1c).

4 When superficial papillary urothelial carcinomas of the bladder are resected transurethrally (TUR), the rate for subsequent development of urothelial carcinomas of a similar biological nature in the normal-appearing bladder mucosa is reported to be 50–80% (Fig. 1d).

5 When cystoprostatectomy (i.e. removal of the bladder and prostate) is carried out for male bladder cancer patients, 4–17% incidences of urothelial carcinomas in the remaining urethra have been described[5] (Fig. 1e). In female bladder cancer patients, involvement of the urethra is reported to occur in 1.4–36% of cases.[6]

After surgical treatment of bladder carcinomas, the incidence of subsequent upper urinary tract carcinomas (of the renal pelvis or ureter) ranges from 0.7 to 4%.[7] Most of these carcinomas are diagnosed 4–6 years after the initial appearance

E-mail: tkakizoe@ncc.go.jp

doi: 10.1111/j.1349-7006.2006.00264.x

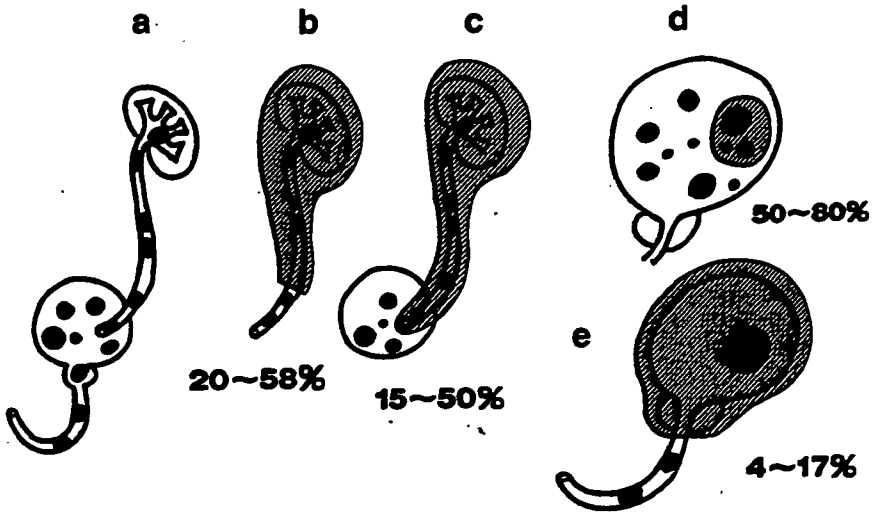

Fig. 1. Clinical findings indicating multifocal tumor development in the urinary tract. Black lesions are original tumors and red lesions are recurrent tumors.

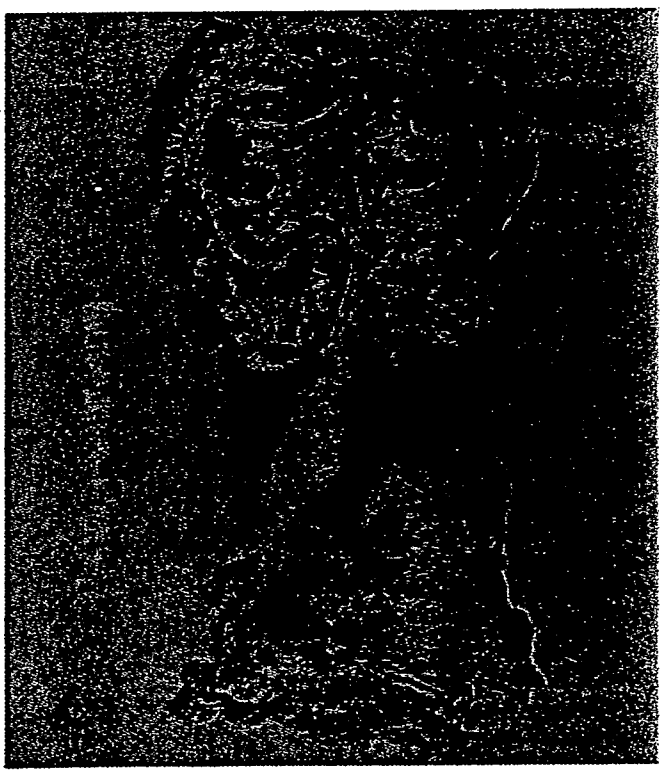

Fig. 2. A case of renal pelvic, ureteral and vesical carcinomas who underwent right nephroureterocystectomy.

of the bladder carcinoma.[8,9] However, the risk is reported to increase to the level of 6–20% (15–22-fold) if the patients suffer from vesico-ureteral reflux.[10]

With upper urinary tract carcinomas, simultaneous bilateral lesions are rare, the estimated incidence being 1–5%.[11] Approximately 2–3% of patients with unilateral upper urinary tract carcinoma experience subsequent contralateral upper urinary tract carcinoma.[12] These clinical data should be taken into serious consideration when we decide on nephroureterectomy or cystectomy and plans for follow up after surgery, and the upper and lower urinary tract and the contralateral upper urinary tract should be assumed to constitute a single clinical unit from the renal pelvis to the urethra.

Field cancerization versus clonal expansion

To explain multifocal carcinoma development in the urinary tract, two theories have been proposed.[13,14] The first is field cancerization, proposed in 1953 by Slaughter *et al.*, which was based on observations of the multicentric development of cancers in the oral cavity, with the high impact of carcinogens and promoting agents being associated with some lifestyle factors.[15] A similar understanding is possible for the urinary tract as the entire urothelium is exposed to carcinogens contaminating the urine. The second hypothesis is that multiple carcinomas in the urinary tract are the result of intraluminal spread from a single lesion, originating from a single transformed cell, namely seeding or implantation of cancer cells at different sites. This phenomenon is also called clonal expansion of multifocal carcinomas. Debates on multiple cancer development have been similar for cancers of the oral cavity,[16] respiratory tract,[17] head and neck,[18] breast,[19] ovary[20] and cervix.[21] Recently, strong molecular evidence has been presented in support of clonal expansion in the epithelium of oral cavity and respiratory tract cases.[16,22]

Many urologists and pathologists have supported the field cancerization hypothesis in the urinary tract, but recent molecular studies have also pointed to a clonal origin for most multifocal urothelial carcinomas. Various molecular analyses have been applied. Sidransky *et al.* investigated X-chromosome inactivation in multiple bladder carcinomas of four female patients and proved that the same allele of the X-chromosome was inactivated in all lesions within the single bladder.[23] Subsequently, Lunec *et al.*[24] and Habuchi *et al.*[25] examined patients having heterotopic synchronous or recurrent urothelial carcinomas in the bladder or upper urinary tract. These carcinomas had identical mutation sites and patterns of p53 gene alteration, indicating the metachronous carcinomas to be derived from the original carcinoma cells due to clonal expansion. Habuchi also reviewed the origin of

doi: 10.1111/j.1349-7006.2006.00264.x

multifocal carcinomas of the bladder and upper urinary tract.[26] Other genetic features that can be used to assess clonal origin are loss of heterozygosity (LOH) and microsatellite alteration patterns, both commonly used as markers of neoplasia.

Stoehr *et al.* analyzed primary carcinomas in 14 cystectomy specimens for p53 protein overexpression by immunohistochemistry and p53 gene mutation by genomic sequencing.[27] They reported detection of p53-mutant cells in histologically normal adjacent or remote mucosa and in preneoplastic urothelial areas in four patients with invasive bladder carcinoma, concluding extensive intraurothelial tumor cell spread.

Evidence of a monoclonal origin and intraepithelial spread has also been provided by Simon *et al.* from comparative genomic hybridization in 32 bladder tumors originating from six cystectomy specimens.[28] Identical *TP53* mutations and protein overexpression were found in tumors from the same individual, as well as in mucosal samples from the continuous areas. The sequence of genomic changes apparently acquired during progression of bladder carcinomas was highly complex and varied within each patient and from tumor to tumor. Early changes included alterations in −17p, +20p, −9p, −9q, +2q34-qter, +12q14-q21, +1q22-q25, −8p22-pter, −5q31-qter and +17q. Subsequent tumor progression was characterized by accumulation of changes in +11q14, −21q, −5q13-q14, +8q22, +10p, −10q22qter and −11p. Cytogenetic variety in multifocal tumors has also been described in support of intraluminal tumor seeding.[29]

It is conceivable that widespread p53-mutated cells in the normal urothelium are generated in the bladder due to carcinogen exposure, and that from these, new tumors later develop with surrounding normal-appearing mucosa having p53 mutations. However, there is no mechanistic explanation for the intraepithelial spread of carcinoma cells to remote normal-appearing mucosa, and it is unrealistic to consider a mechanism due to cell motility.

Although the clonal theory now dominates in explanations of multifocality of urothelial carcinomas, there are also conflicting observations. Cheng *et al.* collected cancer cells by microdissection from 18 cystectomy specimens from female patients and analyzed the X-chromosome-linked human androgen receptor gene.[30] Only 11 of the 18 specimens were informative, with nine exhibiting non-random inactivation of the target locus and seven showing different patterns, indicating field change in these cases. Paiss *et al.* examined X-chromosome inactivation in 45 archival or fresh frozen bladder tumors obtained from 27 female patients using a polymerase chain reaction-based procedure.[31] Polyclonal patterns were observed in 16 of the 45 tumors. Stoehr *et al.* examined multiple samples from four cystectomy specimens for LOH at chromosomes 8p, 9p, 9q and 17p and they observed oligoclonality in two patients.[27] Thus, both hypotheses continue to be discussed, although clonal expansion by intraluminal spread of primary carcinoma appears the dominant explanation for multifocality.

Relationship between papillary carcinoma and nodular carcinoma

Urothelial carcinogenesis has been investigated in various species of animal. A particular focus has been on the histogenesis of lesions in rats treated with the carcinogen *N*-butyl-*N*-(4-hydroxybutyl) nitrosamine (BHBN).[32] Normal urothelium of rats is composed of two to three layers of urothelial cells and when BHBN is given in the drinking water, the mucosal layer becomes hyperplastic at 4 weeks. If BHBN administration is stopped at this point, mild hyperplastic mucosal lesion regresses to the normal state. However, if BHBN treatment is continued, mucosal hyperplasia progresses to papillary growth and papillary carcinomas develop via papillomas (Fig. 3). Large papillary carcinomas may occasionally invade the bladder wall. Usually, papillary carcinomas are multifocal but superficial, indicating bladder carcinoma in rats to be a good model for human papillary bladder carcinoma. With progression, urinary bladders become filled with multifocal urothelial carcinomas and rats die due to massive bleeding. Papillary carcinomas are always induced in rats, irrespective of the strain of animal, the concentration of BHBN, or the carcinogen, with similar findings being reported with *N*-(4-[5-nitro-2-furyl]-2-thizolyl)formamide and *N*-methyl-*N*-nitrosourea.

Urinary bladder carcinogenesis in mice treated with BHBN in the drinking water originates in the normal mucosa (composed of two to three layers of urothelium) and progresses through mild hyperplasia, dysplasia and carcinoma *in situ*, to form large nodular invasive carcinomas[33] (Fig. 4). Bilateral ureters are frequently obstructed due to invasion of carcinomas into the bladder wall, and when advanced, mice die because of renal insufficiency due to hydronephrosis. Because of these features, the bladder carcinomas induced by BHBN in mice offer good models for human nodular invasive bladder carcinoma. Of interest, it has proven impossible to induce multiple papillary carcinomas in any strain of mouse, not with any concentration of BHBN nor any other carcinogen. Thus, there is a clear contrast between the biological and morphological characteristics of bladder carcinomas in rats and mice.

Bladder carcinogenesis in female dogs has been studied extensively by Okajima *et al.* who used these animals to periodically observe the surface of the bladder epithelium directly by cystoscopy.[34] They made capsules of BHBN (80–500 mg/capsule), which were administered once a day. After 4–5 years, papillary superficial bladder carcinomas were induced (Fig. 5), and when these were examined by cystoscopy without further BHBN treatment after more than 10 years, the bladders of the dogs were full of multifocal papillary carcinomas. When dogs were given 500 mg of BHBN daily, nodular invasive carcinomas were induced after approximately 1 year. These findings indicate that bladder carcinogenesis in dogs can be controlled by the concentration and period of BHBN administration in terms of the type of carcinoma (i.e. papillary superficial and nodular invasive bladder carcinoma). Thus, in the various animal species, rats, mice and dogs, the relationship between papillary and nodular carcinomas in the bladder appears to differ.

Morphological and pathological characteristics of human urothelial carcinomas, mainly bladder carcinomas, are a combination of papillary (P), papillonodular (PN), nodular (N) and carcinoma *in situ* (C). On careful analysis of cancerous lesions and normal-looking mucosa of 186 cystectomized specimens by step-sectioning,[35] we classified 17 as C and 80

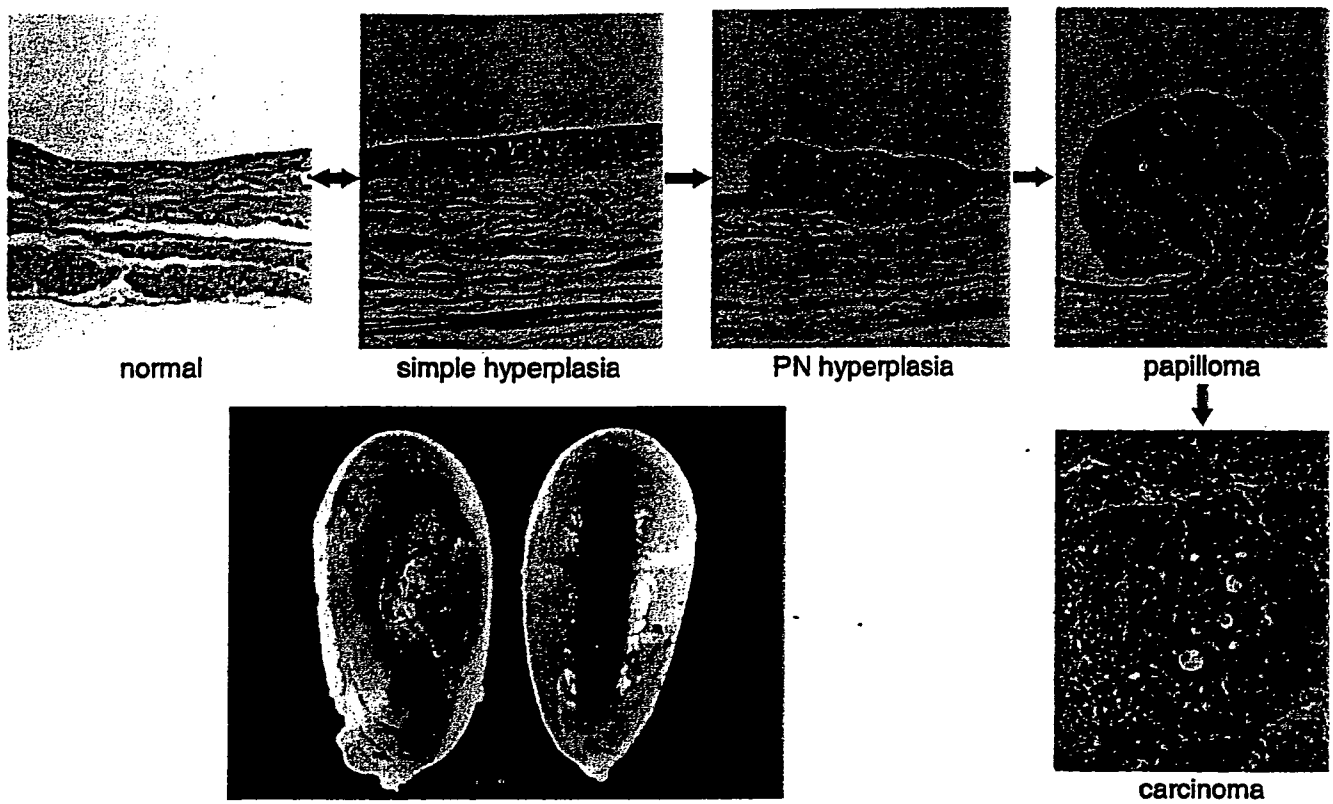

Fig. 3. Histogenesis and progession of papillary carcinomas in rats. (Reproduced with permission from Medical view Co., T. Kakizoe, Development and Progression of Bladder Cancer, 1995.)

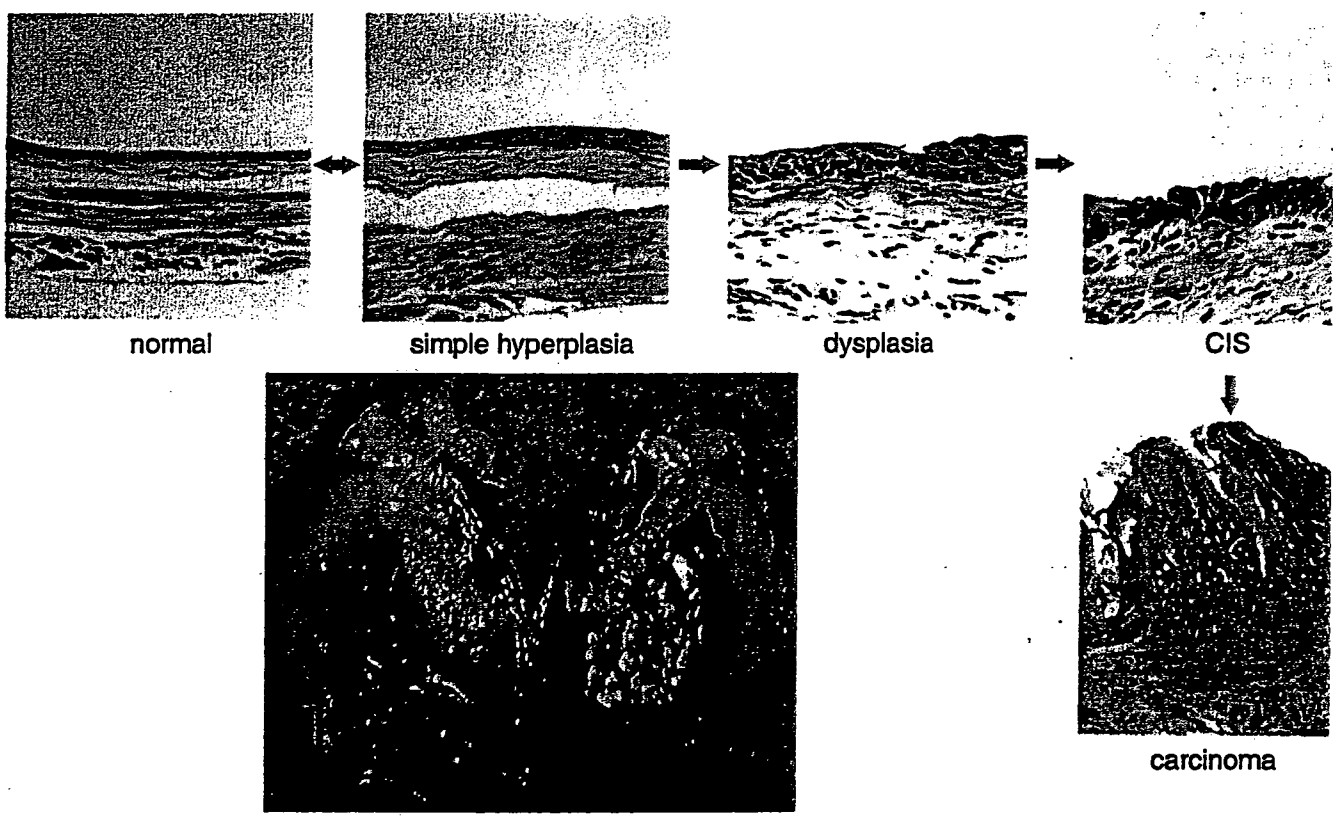

Fig. 4. Histogenesis and progression of nodular invasive carcinoma in mice. (Reproduced with permission from Medical view Co., T. Kakizoe, Development and Progression of Bladder Cancer, 1995.)

doi: 10.1111/j.1349-7006.2006.00264.x

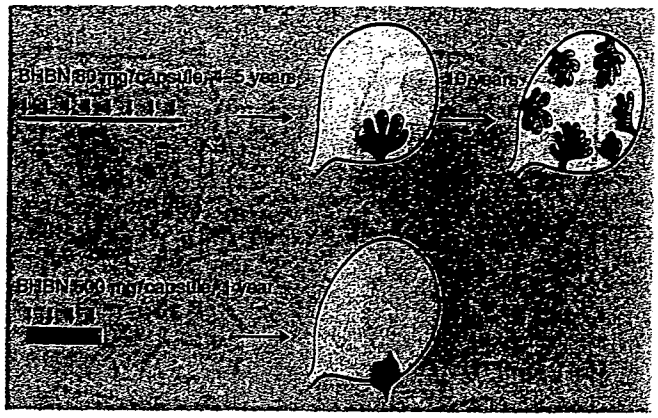

Fig. 5. Development and progression of papillary and nodular carcinomas depending on the concentration and period of administration of *N*-butyl-*N*-(4-hydroxybutyl) nitrosamine (BHBN) in female dogs.[34] (Reproduced with permission from Medical view Co., T. Kakizoe, Development and Progression of Bladder Cancer, 1995.)

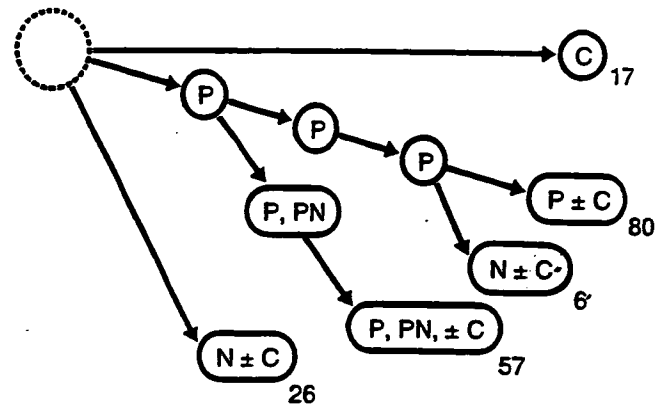

Fig. 6. Conceptual progression routes of papillary (P), papillonodular (PN) and nodular (N) carcinoma, and carcinoma *in situ* (C), in 186 cystectomized specimens examined by step-sectioning.[35]

as P and P + C. Fifty-seven cases featured apparent early changes from P to a mixture of P and N, whereas six showed late development of N with repeated recurrence of P. The findings thus indicated some N to have developed from P as more anaplastic cell populations within a pre-existing low-grade lesion, whereas others arose directly *de novo* from C (Fig. 6). Topographic relationships between P and N in the pT3 group are illustrated in Fig. 7. Figure 8 demonstrates findings for patients having a previous history of repeated recurrence of papillary carcinomas treated by TUR. At the time of cystectomy, all the cystectomized specimens showed a variable degree of coexistence of P, N and C.

Molecular pathways of urothelial carcinogenesis

With papillary superficial and nodular invasive carcinomas, there appear to be differences in molecular pathways as well

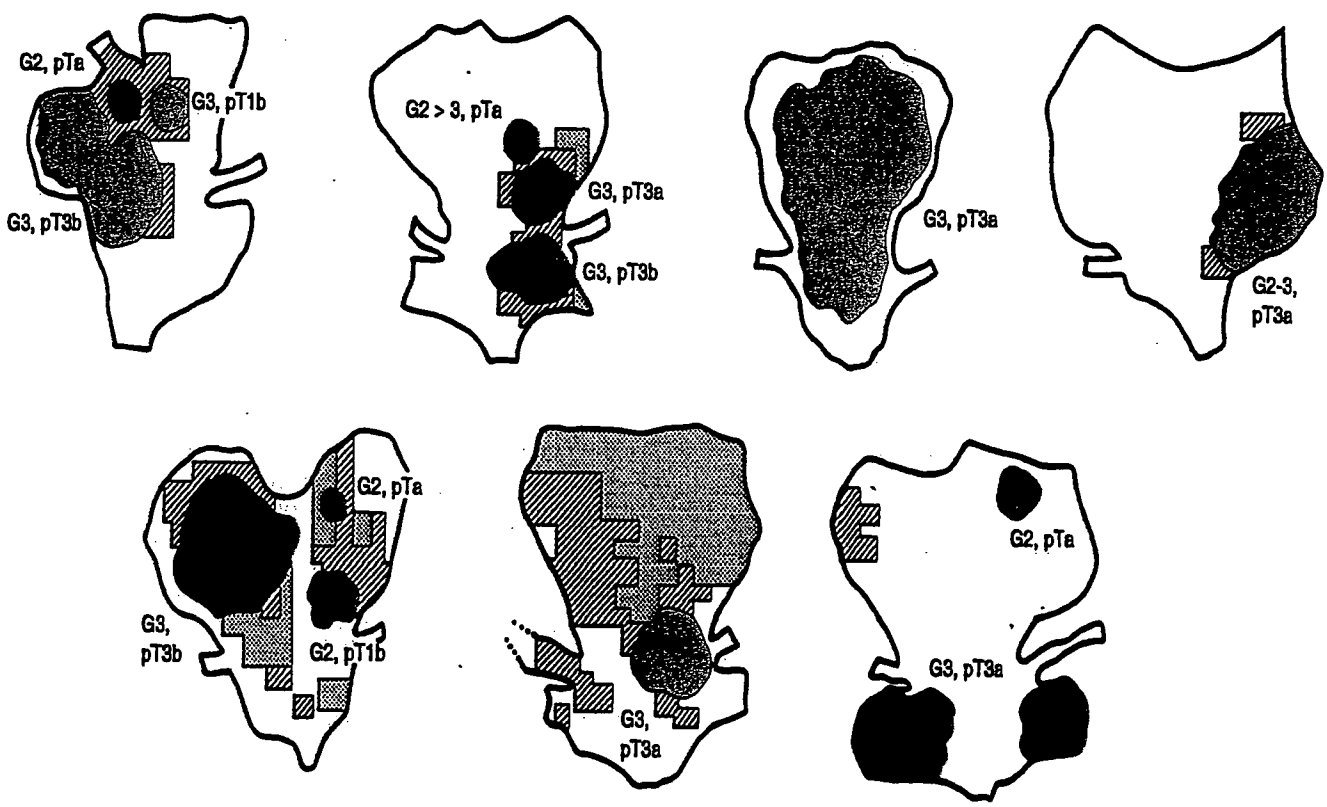

Fig. 7. Cases of pT3 cystectomized specimens indicating coexistence of papillary (P; blue), papillonodular (PN; yellow) and nodular (N; red) carcinoma together with oblique line area (C) and shaded area (dysplasia).[35]

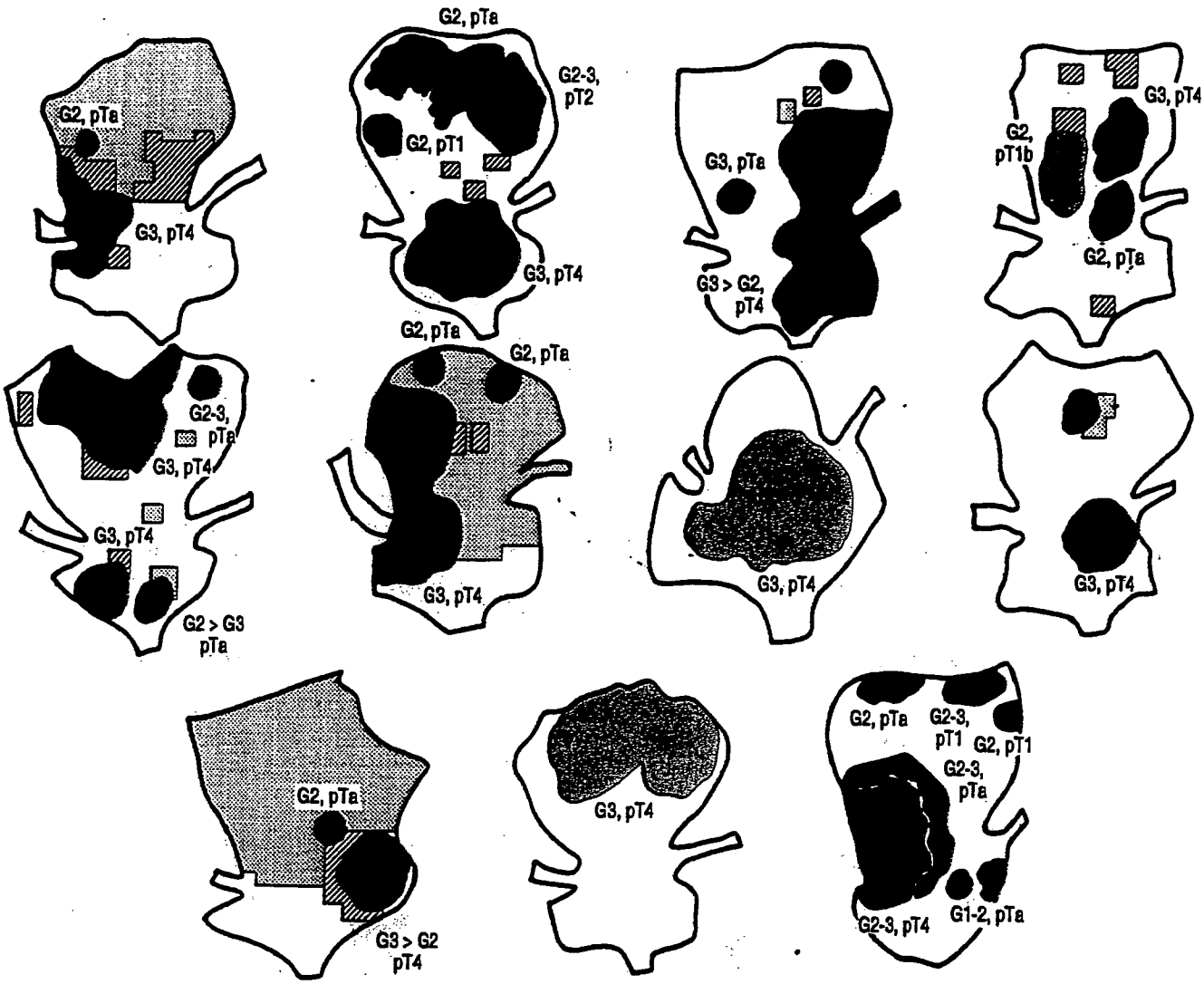

Fig. 8. Eleven cases of cystectomized specimens having histories of multiple transurethral resection for papillary recurrent carcinomas showing variety of stages and morphology in a single bladder.[35]

as morphology[36–38] (Fig. 9). The most common genetic alterations in low-grade papillary urothelial carcinomas are LOH of chromosome 9 and activating mutations of fibroblast growth factor receptor 3 (FGFR3).[39,40] Over 70% of low-grade papillary carcinoma exhibit FGFR3 mutations, but only 10–20% of high-grade invasive carcinomas have FGFR3 mutations, implying a key role for FGFR3 together with mutations of 9p and 9q, specifically for the induction of low-grade papillary carcinomas. Invasive carcinoma is frequently associated with p53 mutations.[41–43]

In addition to the above-mentioned genomic abnormalities associated with urothelial carcinoma, epigenetic alterations also occur during urothelial carcinogenesis. Almost all cells in the human body contain the same sequence of DNA, but cells in different organs during different developmental stages express different genes by epigenetic control of cellular function. This expression control of DNA is achieved by DNA methylation, chromatin structure and transcription factors. DNA can be methylated at cytosine residues adjacent to guanine residues (CpG) and CpG sites are distributed non-randomly throughout the genome, being found as islands in the promoter and exonic regions. Inactivation of tumor suppressor genes is known to occur via promoter hypermethylation, frequently due to DNA methyltransferase 1 (DNMT1). Expression of DNMT1 is increased in tumors and even during the precancerous stages of the urothelium with the development of flat carcinomas *in situ*.[44] Hypermethylation in urothelial carcinogenesis has also been observed in the promoter region of the E-cadherin gene, indicating an association with carcinoma *in situ* and detachment of cells or clusters of carcinoma cells in the urine.[45]

Development and progression of urothelial carcinoma

As is shown in Fig. 1, multifocal transitional cell carcinomas may develop in any region of the urinary tract, from the renal pelvis/ureter to the bladder/urethra.[4,46] Whereas upper urinary

doi: 10.1111/j.1349-7006.2006.00264.x